Regional sea level budget

over 2004-2022

Marie Bouih[1], Anne Barnoud[1], Chunxue Yang[2], Andrea Storto[2],

Alejandro Blazquez[3] , William Llovel[4], Robin Fraudeau[1] and Anny Cazenave[3]

1. Magellium, 31520 Ramonville St Agne, France

2. Institute of Marine Science, National Research Council of Italy, Rome, Italy

3. Université de Toulouse, LEGOS (CNES/CNRS/IRD/UT3), 31401 Toulouse, Cedex, France

4. Univ Brest, CNRS, Ifremer, IRD, Laboratoire d'Océanographie Physique et Spatiale (LOPS), IUEM, F29280, Plouzané, France

Ocean Science

~~submitted~~

~~13 December 2024~~

Revised version, 30 March 2025

Corresponding author : Anny Cazenave

anny.cazenave@univ-tlse3.fr; anny.cazenave@gmail.com

ORCID 0000-0002-2289-1858

ABSTRACT

Closure of the regional sea level budget is investigated over the 2004-2022 time span by comparing trend patterns from the satellite altimetry-based sea level with the sum of contributions, i.e. the thermosteric, halosteric, manometric and GRD (Gravitational, Rotational, and Deformational fingerprints due to past and ongoing land ice melt) components. The thermosteric and halosteric components are based on Argo data (down to 2000m). For the manometric component, two approaches are considered: one using GRACE/GRACE-Follow On satellite gravimetry data, and the other using ocean reanalyses-based sterodynamic sea level data corrected for local steric effects. For the latter, six different ocean reanalyses are considered, including two reanalyses that do not assimilate satellite altimetry data. The results show significantly high residuals in the North Atlantic for both approaches. In a few other regions, small-scale residuals of smaller amplitude are observed and attributed to the finer resolution of altimetry data compared to the coarser resolution of data sets used for the components. The observed strong residual signal in the North Atlantic points to suggests Argo-based salinity errors in this region. However, it is not excluded that other factors also contribute to the reported non-closure of the budget in of this particular area in this region.

1. Introduction

On interannual to decadal time scales, sea level changes in a specific oceanic region arise from several factors. The global mean geocentric sea level rise is primarily driven by ocean warming, land ice melting, and water exchange with continents. Additionally, local and regional effects contribute, including changes in seawater density caused by variations in temperature and salinity (steric effects), as well as the redistribution of ocean water mass through circulation changes (manometric component, Gregory et al., 2019), and variations in atmospheric loading. Furthermore, changes in the solid Earth's gravity, rotation, and deformation (GRD) occur in response to mass redistributions from past and present-day land ice melt and land water storage changes. These GRD factors include two components : the Glacial Isostatic Adjustment (GIA) effect, which stems from the last deglaciation, and GRD fingerprints, which are associated with contemporary land ice melting and, to a lesser extent, changes in land water storage (Gregory et al., 2019).

In terms of global average, the rate of sea level rise is dominated by ocean warming via thermal expansion of seawater, and land ice melting (from glaciers, Greenland and Antarctica ice sheets), in response to global warming (e.g., Cazenave et al., 2018, Nerem et al., 2018, IPCC, 2019, 2021, Cazenave and Moreira, 2022, Horwath et al., 2022, IPCC, 2019, 2021 Llovel et al., 2023). The spatial variations of the rate of sea level rise mainly result from steric effects, with the thermosteric contribution being generally dominant (e.g., Stammer et al., 2013, Hamlington et al., 2020), except in the Arctic where the halosteric effect is important (e.g., Carret et al., 2017, Tajouri et al., 2024).

Focusing on trends, mMany studies have computed the global mean sea level budget over the altimetry era (i.e., since the early 1990s) by comparing the global mean sea level rise with the sum of the thermal and mass components from independent observing systems (e.g., Dieng et al., 2017, Nerem et al., 2018, WCRP, 2018, Horwath et al., 2022, Chen et al., 2018, 2020, Barnoud et al., 2021, 2023, to focus only on the most recent publications). These studies have shown that at least until 2016, the global mean sea level budget is closed within the data uncertainties. In recent years, some discrepancy has been observed between the altimetry-based global mean sea level and the sum of the Argo-based steric and gravimetry-based mass components (e.g., Chen et al., 2020, Barnoud et al., 2021, 2023, Mu et al., 2024), especially when using the Gravity Recovery And Climate Experiment (GRACE) and GRACE Follow-On (GRACE-FO) satellite data to estimate the total mass contribution to sea level change, instead of individual mass contributions (i.e., glaciers, Greenland and Antarctica ice sheets, land

80   waters and atmosphere water vapor). At regional scale, the closure of the sea level budget

81   has been less studied so far. A few recent studies have assessed the closure of the sea level

82   budget at ocean the basin-scale, over the altimetry era (e.g., Rietbrock et al., 2016, Frederiske

83   et al., 2016, 2018, 2020; Hamlington et al., 2020, Royston et al., 2020, Camargo et al., 2023,

84   Mu et al., 2024). The regional ocean mass budget has also been investigated (Ludwigsen et

85   al., 2024). Closure of the regional budget is only observed in some regions but not everywhere.

86   For example, using altimetry, gravimetry and Argo data over 2005-2015, Royston et al. (2020)

87   concluded that the regional budget cannot be closed in the Indian-South Pacific region.

88   Similarly, Camargo et al. (2023) also found non-closure of the regional sea level budget in a

89   number of oceanic areas. Using machine learning techniques, these authors were able to

90   identify processes not well captured by the observations that are considered to assess closure

91   of the regional sea level budget.

92   In the above studies, closure of the regional budget was assessed by averaging the data either

93   at ocean basin-scales or smaller sub-basin scales. In the present study, we revisit the regional

94   sea level budget over the GRACE/Argo era (starting in 2004) at the local scale, without

95   averaging the data at the basin-scale. After removing the global mean trend of each

96   component, we focus on the spatial trend patterns, with a resolution of about 300 km, as

97   allowed by the gridded data sets considered, an approach not applied in the previous studies.

98   This approach avoids compensation of spurious positive/negative sub-basin trend patterns

99   and allows for more precise identification of the areas where the sea level budget is not closed.

100   For this investigation, we use gridded satellite altimetry data for the observed sea level

101   changes and Argo data to estimate the thermosteric and halosteric sea level changes. For the

102   manometric component, two types of data are considered: satellite gravimetry data from the

103   GRACE and GRACE FO missions as well as ocean reanalyses to estimate the redistribution

104   of water mass already in the ocean (following the same approach as in Camargo et al., 2023,

105   i.e., estimating sterodynamic sea level changes corrected for local steric effects; see section

106   3). The study period covers the period from January 2004 to December 2022 (although some

107   data sets end in December 2019; section 3).

108

109 2. Brief overview of the sea level components at
110 regional scale

111 2.1. Steric component

112 The steric component includes the effects of ocean temperature and salinity changes. Remote
113 surface wind forcing, heat and freshwater fluxes associated with variations in the overlying
114 atmospheric state are the two main forcing mechanisms causing steric changes (Stammer et
115 al., 2013, Roberts et al., 2016). Wind forcing modifies the ocean circulation which further
116 redistributes heat and water masses. It is the dominant mechanism of interannual to decadal
117 steric changes in many regions, particularly in the tropics (e.g., Timmermann et al., 2010;
118 Merrifield and Maltrud, 2011; Piecuch and Ponte, 2014; England et al., 2014). Wind forcing
119 can also play a role in the extra tropics and at high latitudes (Roberts et al., 2016). Buoyancy
120 forcing, i.e. surface air-sea fluxes of heat and freshwater (due to surface warming and cooling
121 of the ocean, and exchange of freshwater with the atmosphere and land through evaporation,
122 precipitation, and runoff) is important in mid to high latitudes, e.g., in the North Atlantic Ocean
123 (Gulf Stream and North Atlantic subpolar gyre) (Roberts et al., 2016).

124 Over the altimetry era, regional sea level patterns are dominated by steric changes. In most
125 regions, the thermosteric component by far dominates the halosteric one, except in the North
126 Atlantic Ocean (Llovel and Lee, 2015) and in high latitude areas, e.g., in the northeast Pacific,
127 and particularly in the Arctic (e.g., Carret et al., 2016; Ludwigsen et al., 2022, Tajouri et al.,
128 2024). On interannual to multidecadal time scales, the spatial trend patterns in (thermo) steric
129 sea level are still largely influenced by basin-scale internal climate modes of variability, e.g.,
130 El Niño-Southern Oscillation (ENSO), Pacific Decadal Oscillation (PDO), Atlantic Multidecadal
131 Oscillation (AMO), North Atlantic Oscillation (NAO) and Indian Ocean Dipole (IOD). Wind
132 stress changes on such time scales are indeed directly related to climate modes (Han et al.,
133 2017). For example, sea level in the tropical Pacific oscillates from west to east with ENSO
134 (with high/low sea level in the eastern/western part during El Niño/La Niña events), in response
135 to wind-forced propagating waves. In the North Atlantic, surface wind and heat flux partly drive
136 interannual to decadal sea level fluctuations and are associated with the NAO (but changes
137 in the Atlantic Meridional Ocean Circulation also contribute) (Han et al., 2017). In the tropical
138 Indian Ocean, interannual to decadal variability in sea level is strongly influenced by ENSO
139 and the IOD (Han et al., 2017, 2019).

2.2. Manometric component

The total regional manometric sea level change has two components: (1) essentially results from spatial redistribution of water mass already in the ocean by the ocean circulation, plus the total water mass added to the ocean (the latter being called barystatic component; Gregory et al., 2019), due to land ice melt and to the exchange of water with the continents, and (2) the spatial redistribution of water mass by the ocean circulation (Gregory et al., 2019). The barystatic contribution nearly uniformly covers the oceanic domain rapidly (within a few weeks) via a barotropic global adjustment occurring on short time scales (Lorbacher et al., 2012). Because the global mean trend of each component of the regional sea level budget is removed in this study, the barystatic component (i.e., the global mean ocean mass change) disappears. Compared to steric changes, the manometric sea level change due to water mass redistribution (barystatic contribution removed), plays a smaller role on interannual to decadal time scales, but can be sizeable (e.g., Dangendorf et al., 2021, Wang et al., 2022), in particular at high latitudes and over shallow continental shelves (e.g., Forget and Ponte, 2015; Carret et al., 2021).

2.3. Atmospheric loading

On seasonal and longer time scales, sea level responds as an inverted barometer to atmospheric loading (Wunsch and Stammer, 1997) i.e. the sea surface height increases (decreases) by 1 cm if the local surface pressure decreases (increases) by approximately 1 mbar. The atmospheric loading component is quite small compared to the thermosteric one, but it is non-negligible at high latitudes (e.g., in the Arctic Ocean where it can reach 0.3 mm/yr equivalent sea level on interannual to decadal time scales, Proshutinski, 2004). Atmospheric loading can be estimated using e.g. surface pressure data from atmospheric reanalyses.

2.4. Gravity, Earth Rotation, and solid Earth Deformations (GRD)

The response of the solid Earth to past and present-day water mass exchange between continents and oceans causes global and regional sea level changes. The GIA results from the ice and water mass redistribution of the last deglaciation. Its effect depends on the Earth's mantle viscosity and deglaciation history. The response of the solid Earth to ongoing land ice melt essentially depends on the elasticity of the lithosphere and mantle, as well as on the amount and location of ice mass loss. These mass redistributions induce changes in the gravity, rotation, and visco-elastic deformations of the solid Earth (Mitrovica et al., 2001; Milne et al., 2009; Stammer et al., 2013). These are the so-called GRD (Gravity, Earth Rotation,

172 and solid Earth Deformations) fingerprints (Gregory et al., 2019). In the literature, the GRD
173 contribution is often separated into the one resulting from the GIA (last deglaciation) and the
174 contemporary GRD effects, the latter referring to mass redistributions due to present-day
175 land ice melt and land water storage variations. In terms of global average, the GIA effect on
176 the absolute sea level change is around -0.3 mm/yr (Peltier, 2004; Tamisiea, 2011, Caron et
177 al., 2018). Its regional signature is mostly uniform, except in formerly glaciated high-latitude
178 regions. The contemporary GRD fingerprints produce complex regional patterns in sea level
179 change : sea level drops near the melting bodies but sea level rises in the far field (e.g., along
180 the northeast coast of North America). Several studies have theoretically computed the impact
181 of contemporary GRD changes on relative and absolute sea levels, by solving the sea level
182 equation, either assuming a priori current ice sheet mass loss (e.g., Mitrovica et al., 2001,
183 Tamisiea, 2011, Spada, 2017), or using realistic ice mass loss based observations from the
184 GRACE satellite gravimetry mission (Adhikari et al., 2019). Note that the sea level fingerprints
185 associated with the GIA and the contemporary GRDs are usually expressed in terms of linear
186 trends and have a small amplitude (<0.5 mm/yr except around the ice sheets where the
187 magnitude increases to ~1 mm/yr), compared to the observed regional sea level and steric
188 sea level trends of several mm/yr magnitude. However, with the expected increase of land ice
189 melt in the coming decades, the contribution of the contemporary GRD fingerprints to regional
190 sea level trends may become increasingly significant.
191

192 3. Data and methods

193 3.1. Data

194 3.1.1 Total Altimetry-based total sea level

195 Total sSea level is routinely observed by satellite altimetry. In this study, we use the daily 1/4°
196 x 1/4° gridded sea level anomaly data version DT2021 from the Copernicus Climate Change
197 Service (C3S) (https://climate.copernicus.eu). To ensure the long-term stability of this
198 altimetry-based data, C3S sea level anomalies rely on two simultaneous satellite missions at
199 any given time: the successive reference missions (TOPEX/Poseidon, Jason-1, Jason-2,
200 Jason-3, and Sentinel-6 Michael Freilich) plus an auxiliary mission from the global
201 constellation. The dataset is corrected for TOPEX-A altimeter drift (Ablain et al., 2017), as well
202 as for the Jason-3 radiometer drift that impacts the wet troposphere correction (Brown et al.,
203 2023). The dataset covers the period from January 1993 to December 2023. The C3S dataset
204 is corrected for GIA using the ICE6G-D model (Peltier et al., 2018). The Total sea level

205 uncertainty in the rate of the global mean sea level is estimated to 0.3 mm/yr (Ablain et
206 al.,2019, Guérou et al., 2023). At regional scale, trend uncertainties are larger, on the order of
207 1 mm/yr especially in coastal areas (Prandi et al., 2021).

3.1.2 Steric sea level

209 We compute use the Argo-based steric sea level data from the Roemmich-Gilson Argo
210 climatology offrom the Scripps Institution of Oceanography (SIO) which provides monthly
211 gridded data of temperature T and salinity S at a 1° x 1° resolution and 58 depth levels until
212 2000 meters (Roemmich and Gilson, 2009) (data downloaded in July 2024). The choice for
213 the SIO product is motivated by the fact that its post-processing corrects for the salinity drift
214 reported in Argo floats since 2015, which misleads to a spurious increase reported in the global
215 mean salinity (Wong et al., 2023; Liu et al., 2020, 2024; Ponte et al., 2021). This salinity drift
216 has a significant impact on the sea level budget closure (Chen et al., 2020; Barnoud et al.,
217 2021). The SIO processing methodology considers the most up-to-date delayed-mode Argo
218 profiles which have been meticulously quality-controlled by a scientist (typically within 1-2
219 years after the float transmits the data). In addition, the SIO processing adjusts the real-time
220 Argo profiles (which have passed through automatic quality-control typically within 24 h) to fit
221 the WOCE (World Ocean Circulation Experiment) global hydrographic climatology. This
222 specific processing has the benefit of removing the salinity drift in the SIO steric sea level data
223 (Liu et al., 2024). The dataset covers the period from January 2004 to December 2022, within
224 the 0–2000 m depth range, and the latitudes between 66°S and 66°N.
225 In this study, the deep ocean's contribution to steric sea level is not considered due to its small
226 magnitude (on the order of 0.1 mm/yr) and possibly high uncertainty (e.g., Purkey and
227 Johnson, 2010). Based on the deep Argo profiles, Lele and Purkey (2024) estimated the deep
228 ocean steric sea level rise (temperature and salinity contribution) being 0.13 ± 0.16 mm/yr in
229 the south Pacific Ocean over 2014-2023, confirming the small contribution of the deep steric
230 sea level rise.
231 The thermosteric, halosteric and total steric sea level changes are computed from the gridded
232 temperature and salinity data using the Lenapy library (https://github.com/CNES/lenapy) from
233 the Centre National d'Études Spatiales (CNES), based on the Gibbs seawater oceanography
234 toolbox of the 2010 Thermodynamic Equation Of Seawater (TEOS-10).

3.1.3 Manometric sea level

236 The manometric sea level change is estimated using two independent methods.
237 The first approach relies on satellite gravimetry data from the GRACE mission (2002-2017,
238 Tapley et al., 2019) and GRACE-FO mission (launched in 2018, Landerer et al., 2020), which

239   enables to estimate changes in the Earth's gravitational field linked to mass redistribution,
240   including the regional sea level variations due to GRD effects. Two kinds ~~sources~~ of GRACE
241   solutions are considered:

242   - (1) An ensemble mean of so-called mass concentration (mascon) solutions (update
243   from Blazquez et al., 2018). We use the latest GRACE and GRACE-FO Release 6
244   mascon solutions from the Center for Space Research (CSR; Save et al., 2016), Jet
245   Propulsion Laboratory (JPL; Watkins et al., 2015), and Goddard Space Flight Center
246   (GSFC; Loomis et al., 2019). These mascon solutions are corrected for the GIA effect
247   using the ICE6G-D model (Peltier et al., 2018), as well as for the geocenter motion
248   using the correction from Sun et al. (2016). The effects of the ocean dynamics and
249   atmospheric loading are restored using the GAD product derived from the Atmosphere-
250   Ocean Dealiasing (AOD1B) models (Flechtner et al., 2015, Dobslaw et al., 2017). To
251   retrieve the ocean mass contribution comparable to the difference between altimetry
252   and Argo, the effect of the mean atmospheric pressure over the ocean is removed
253   using the spatial mean of the GAD product at each month (Chen et al., 2019). The
254   manometric component is estimated as the mean of these three gridded ocean mass
255   products, which are given in equivalent water height.

256   - (2) An ensemble of 60 spherical harmonic (SH) solutions. This ensemble is derived
257   from the manometric GRACE-based products (DOI: 10.24400/527896/a01-2023.011
258   version 4.0) and distributed at AVISO+ (https://aviso.altimetry.fr). This product allows
259   for uncertainty estimates linked to various stages of GRACE and GRACE-FO data
260   processing (Blazquez et al, 2018). This ensemble of 60 solutions results from the
261   combination of five processing centres, three C20/C30 (spherical harmonics of degree
262   2 and 3 of the gravity field potential) estimates, ~~and~~ two GIA models (ICE6G-D from
263   Peltier et al., 2018 and the model from Caron et al., 2018), and two levels of denoising
264   and decorrelation kernel filtering. The geocenter motion is corrected with a model
265   based on the approach developed by Sun et al. (2016) and Swenson et al. (2008).
266   Each ensemble member is also corrected for the water vapor mass in the atmosphere
267   using the C0 from GAA (Chen et al, 2019). For each ensemble member, atmospheric
268   loading over the ocean is restored using the GAD products (Flechtner et al., 2015,
269   Dobslaw et al., 2017) to correct for the inverse barometer effect, aligning the ocean
270   mass variations with satellite altimetry data in which atmospheric loading is already
271   accounted for.

272   The two sets of GRACE solutions~~data~~ used here cover the period from January 2004 to
273   December 2022. In case of missing monthly data, a linear interpolation is applied to
274   account for the data gaps. However, no interpolation is performed for the ~one-year gap
275   between GRACE and GRACE-FO.

276

277   The second approach follows Camargo et al. (2023) method which derives the manometric
278   sea level change from ocean reanalyses. Ocean models provide the sterodynamic sea level
279   change, i.e., the sea level change due to changes in ocean density and circulation, with the
280   inverse barometer correction applied (Gregory et al., 2019; Storto et al., 2024). The
281   corresponding manometric component is derived by ~~subtracting the local steric effect to~~
282   ~~correcting~~ the reanalysis-based sterodynamic sea level, ~~by the local steric effec~~t and adding
283   the contemporary GRD fingerprints (Gregory et al., 2019; Camargo et al., 2023). It is the
284   approach followed here.
285   We consider six different ocean reanalyses with different characteristics as listed in Table 1.
286   GLORYS, C-GLORS, ORAS5, and FOAM use the NEMO (Nucleus for European Modelling of
287   the Ocean) ocean model and assimilate satellite altimetry-based sea level data. The SODA
288   reanalysis is based on the MOM (Modular Ocean Model) developed by NOAA (National
289   Oceanographic and Atmospheric Administration, USA) and does not include altimetry data.
290   All reanalyses have a spatial resolution of 0.25°. In order to assess the regional sea level
291   budget with another manometric component independent of satellite altimetry data, we also
292   consider an ensemble reanalysis at lower resolution and without altimetry data assimilation
293   (called CIGAR; see Table 1). This variety of reanalyses offers the opportunity to evaluate the
294   degree of consistency of the manometric signal from reanalysis-based products.

295

296   *Table 1: Characteristics of the six ocean reanalyses used in this study to estimate the*
297   *manometric sea level change patterns independently from GRACE and GRACE-FO data.*

Reanalysis	Ocean model, Spatial Resolution, End date	Data assimilation of altimetry-based sea level data	References
GLORYS (MOI)	NEMO, 0.25°, 2022	Yes	Garric and Parrent (2017)
C-GLORS (CMCC)	NEMO, 0.25°, 2022	Yes	Storto and Masina (2016)
ORAS5 (ECMWF)	NEMO, 0.25°, 2022	Yes	Zuo et al. (2019)

FOAM (UK Metoffice)	NEMO, 0.25°, 2022	Yes	Blockley et al. (2014)
SODA (Version 3.4.2, U.Maryland)	MOM4, 0.25°, 2019	No	Carton et al. (2018)
CIGAR (CNR-ISMAR)	NEMO, 1°, 2022	No	Storto and Yang (2024)

298

299 To compare the manometric component derived from ocean reanalyses with the one based
300 on GRACE and GRACE-FO, we added the contemporary GRD contribution to the reanalysis-
301 based manometric sea level change. We used the sea level fingerprint data from Adhikari et
302 al. (2019), which provides monthly contemporary GRD fingerprints at a 0.5° x 0.5° resolution.
303 Because the Adhikari et al. (2019) data set ends in 2016, we linearly extrapolated the GRD
304 fingerprints up to 2022 and added the corresponding trends to the ocean reanalyses-based
305 manometric trends.

306 3.2. Method

307 Systematic corrections for both atmospheric loading and GIA effects are applied to altimetry-
308 based and satellite gravimetry datasets, even though different models are used in each
309 dataset. The MOG2D (Carrere and Lyard, 2003) and inverse barometer model is used for
310 altimetry data (www.aviso.altimetry.fr), while the GAD product, is used for GRACE and
311 GRACE-FO data (see section 3.1.3). Likewise, the GIA corrections rely on the ICE6-G model
312 for altimetry (Peltier et al. 2018), while GRACE datasets use either ICE6-G (Peltier et al. 2018)
313 or Caron et al. (2018) models.

314 All datasets were spatially interpolated onto a 1° x 1° grid and were averaged on a monthly
315 basis. For spatial consistency, a common masking technique was applied to all gridded
316 components. This mask covers latitudes from 66°S to 66°N, excludes inland seas, and omits
317 coastal regions where the distance from land is less than 300 km.

318 All datasets span from January 2004 to December 2022, except for the oceanic reanalyses-
319 based manometric components for which two study periods were considered, depending on
320 the dataset availability: January 2004-December 2019 and January 2004-December 2022.

321 Finally, seasonal signals (annual and semi-annual) were removed at each grid mesh of each
322 data set through a simple least-squares adjustment of 6-month and 12-month sinusoids, and

323 a 3-month Lanczos filter was applied locally to each dataset to remove high frequency signals.

324 The global mean trend of each dataset computed over the study period was also removed

325 before constructing the spatial trend maps.

326 For each gridded data set, we computed a trend uncertainty~~error~~ map.

327 For the altimetry data, we used the trend uncertainties~~errors~~ provided by Prandi et al. (2021).

328 These are based on a statistical computation which estimates via a generalized least-squares

329 approach the total uncertainty of regional sea level trends due to all sources of errors affecting

330 the altimetry-based sea level measurements (i.e., orbit, range, geophysical corrections and

331 intermission bias). In this approach, individual variance-covariance matrices describing ~~space~~

332 ~~and~~ [1]time correlated errors are computed for each source of uncertainty~~type of error~~.

333 Uncertainties~~Errors~~ from all sources are further combined by summing~~ed~~ up the

334 variances~~together~~. Regional sea level trend uncertainties~~errors~~ provided by Prandi et al.

335 (2021) with this method, applied to altimetry-based sea level grids of 2°x2° resolution over

336 1993-2019 are on the order of 1 mm/yr or less (1-sigma). The largest errors are located along

337 the continental coastlines.

338 Since the SIO temperature and salinity data are not provided with uncertainties~~errors,~~, we

339 computed trend uncertainties~~errors~~ for the thermosteric and halosteric components by

340 considering the dispersion between two thermosteric/halosteric products: the SIO product

341 used here and the EN4 T/S database, version 2.2

342 (https://www.metoffice.gov.uk/hadobs/en4/download-en4-2-2; Good et al., 2013). We

343 estimated the thermosteric and halosteric trend uncertainty at each grid mesh from the

344 dispersion between the two data sets (SIO and EN4) around the mean. For the total steric,

345 thermosteric and halosteric trend uncertainties ~~errors~~ were quadratically combined.

346 As the ensemble mean of the 60 SH GRACE solutions is provided with trend

347 uncertainties,~~errors~~ (adapted from Blazquez et al., 2018), these are used here for both

348 GRACE-based manometric components (i.e., the ensemble mean mascon and the SH

349 solutions).

350 Finally, for the uncertainties ~~errors~~ of the residual trend map (based on GRACE for the

351 manometric component), we quadratically combined trend uncertainties ~~errors~~ of all

352 components at each grid mesh.

353 Please note that the reanalyses used here do not provide uncertainty estimates.

354 In Figure S1 of the Supplementary Information (SI) are shown trend and associated trend

355 uncertainty ~~error~~ maps for the altimetry-based sea level, components and residuals. Note that

356 for altimetry-based sea level and components, the trend uncertainty ~~error~~ map includes the

global mean trend uncertainty (of smaller magnitude than the regional trends). Uncertainties correspond to 1-sigma errors.

4. Results: Regional sea level budget with GRACE and Argo

4.1. Trend patterns in observed sea level, components and residuals

Figure 1 shows the maps of altimetry-based sea level trends, of the GRACE- and Argo-based component trends, and of the residual trends (i.e., trend differences between altimetry-based sea level and sum of components). Hatched areas on the figures correspond to regions where the signal to noise ratio is not significant. This is based on comparing at each grid mesh, the observed trend with the trend uncertainty error (shown in Figure S1). From Figure 1, we note that except for the elongated negative pattern east of the Philippines in the western tropical Pacific, the altimetry-based sea level trends are significant everywhere. Concerning the GRACE-based manometric component, trends are not significant over a large portion of the northeast Atlantic. The halosteric map displays a few regions where the trends are not significant. Most are located in the southern hemisphere. Accordingly, these translate into the total steric map. Finally, the residual trend map shows that the signal is significant essentially in areas where the residual trends are positive. Over several hatched areas, the residual trends are not significantly different from zero. This concerns most of the Pacific Ocean and a portion of the South Atlantic Ocean.
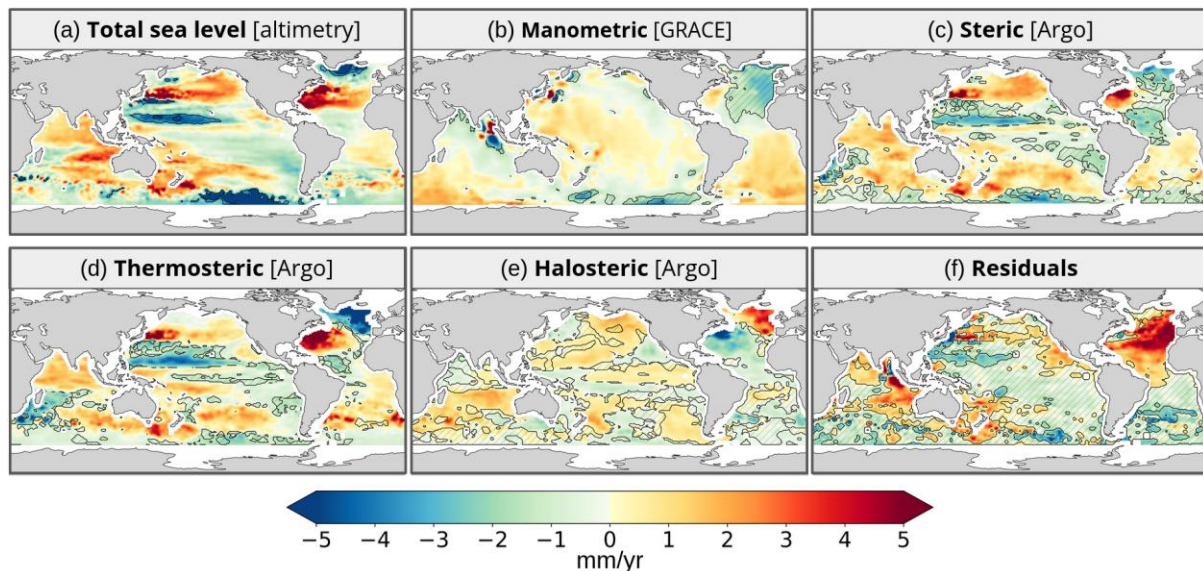
Figure 1: Sea level trends over January 2004 to December 2022 in total ~~observed~~ altimetry-based sea level (a), manometric componen~~t~~t based on GRACE mascons (b),~~Argo-based total~~ steric (c)~~s (b, c, d: GRACE-based manometric, Argo-based~~ thermosteric and ~~Argo-based~~ halosteric components (d and e)~~sea level)~~ and budget residual trends (observed sea level minus sum of components) (~~f~~e). The hatched areas correspond to regions where the signal trend value is not significant compared to the corresponding trend uncertainties.

Visual inspection of Figure 1 confirms earlier findings, i.e., the observed regional trend patterns are dominated by the thermosteric trend patterns (as expected; e.g., Stammer et al., 2013; Hamlington et al., 2020; Cazenave and Moreira, 2022). In the North Atlantic, thermosteric and halosteric trends have opposite signs. Except for two spots of high signal along the coasts of north Indonesia and Japan due to the solid Earth response to the Sumatra and Tohoku earthquakes in 2004 and 2011 respectively (not removed here), t~~T~~he manometric trend map is dominated by large-scale patterns, positive over almost the whole Pacific, as well as over the south Atlantic Ocean and southwest Indian Ocean. The absence of small-scale patterns likely results from the lower resolution of GRACE and Argo data compared to other data sets.

The residual trend map shows that in many regions, the sum of components ~~does not~~ cancels out the observed trend~~s~~s. This is the case over most of the Pacific Ocean, part of the South Atlantic Ocean and southwest Indian Ocean. In these regions, the residuals are not significantly different from zero, which suggests that the regional sea level budget can be considered as closed.

In the eastern Indian O~~o~~cean, along the coast of North Indonesia, the positive residuals result from the solid Earth signal due to the 2004 Sumatra earthquake, not removed from the

GRACE-based manometric component. The same is true for the positive residuals east of Japan and associated with the 2011 Tohoku earthquake. Besides these two regions, it is in the Northeast Atlantic Ocean that where a the strongest positive residual trends are is observed. In this region, altimetry-based and thermosteric sea level displays positive trends in the western part and negative trends south of Greenland while . The opposite patterns are seen in the thermosteric and halosteric component.

The strong residual signal in the North Atlantic is discussed in detail in section 6.
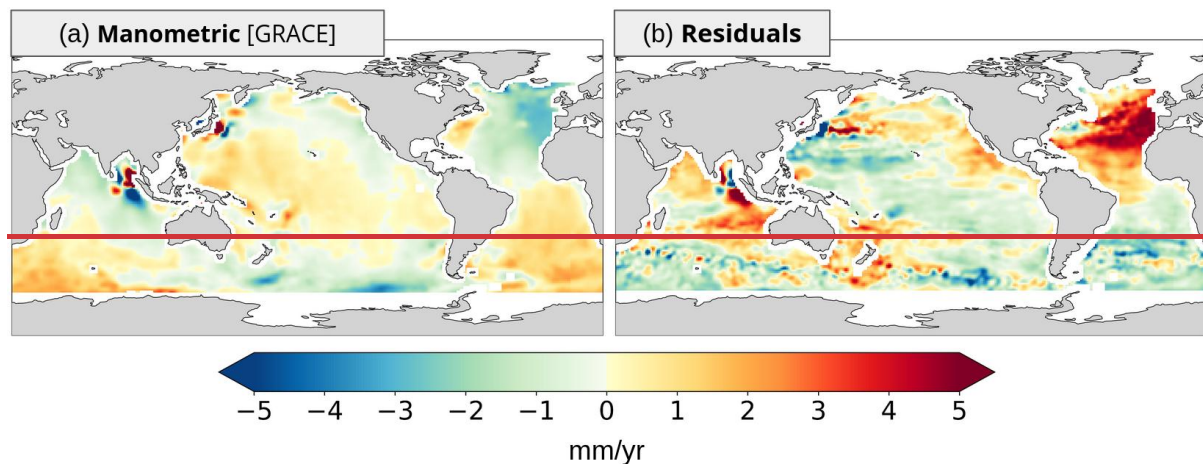
Figure 2: Large-scale trend patterns in the GRACE-based manometric sea level (a) and residuals (b).

4.2. GRACE data assessment

In this section, we explore the impact of the geocenter and GIA corrections applied to GRACE data on the residual trend map, considering that these two corrections remain imperfectly known (Blazquez et al., 2018). For that purpose, we decomposed the sea level budget components into spherical harmonics and computed the residuals for various configurations of low degree harmonics (see Figure S2 and Ttable S1 in the Ssupplementary Iinformation, SI). Figure S21 and Table S1 show that degree 1,0 (related to the geocenter motion) and degree 2,1 (related to polar motion and GIA correction) harmonics contribute to the high positive residuals observed in the North Atlantic Ocean.

GRACE data are classically corrected for the geocenter motion when compared with altimetry data, in order to moving GRACE observations from the centre of mass to the centre of figure of the reference system, in which the altimetry-based sea level is supposed to be also

427 expressed after correcting the satellite orbits for the geocenter motion (Alexandre Couhert,
428 personal communication).

429 Using the ensemble of 60 spherical harmonic solutions described in Section 3.1, we
430 constructed an alternative ensemble of 60 solutions without applying the correction for the
431 geocenter motion, i.e. keeping the GRACE observations in the centre of mass reference
432 system. Comparing these two ensembles of solutions allows us to assess the influence of the
433 geocenter correction on the manometric component and, consequently, on the residuals of
434 the sea level budget. Figure 2 shows the impact of the geocenter correction on the
435 manometric trends as well as on the associated residual trends. Not correcting for the
436 geocenter motion reduces the residuals observed in the North Atlantic Ocean but increases
437 the residual trends elsewhere, with larger residuals in almost all other ocean basins. Thus,
438 even if the Sun et al. (2016)'s geocenter correction may not be optimal, it minimizes the
439 residual trends, except in the northeast Atlantic Ocean. This questions the actual referential
440 of altimetry data and the consistency of the processing between satellite altimetry and satellite
441 gravimetry data. Normally, this should be consistent as altimetry-based sea level is supposed
442 to be expressed in a center of figure reference frame, like the GRACE data after correcting for
443 the geocenter term. However, the way the geocenter is corrected in the orbits used in the
444 altimetry-based processing could still be an issue (Alexandre Couhert, personal
445 communication). Besides, if no geocenter correction is applied, the GRACE-based
446 manometric component displays large scale signals not observed by altimetry data, so that
447 the corresponding residual trends (Figure 2d) also present unrealistic large-scale signals.
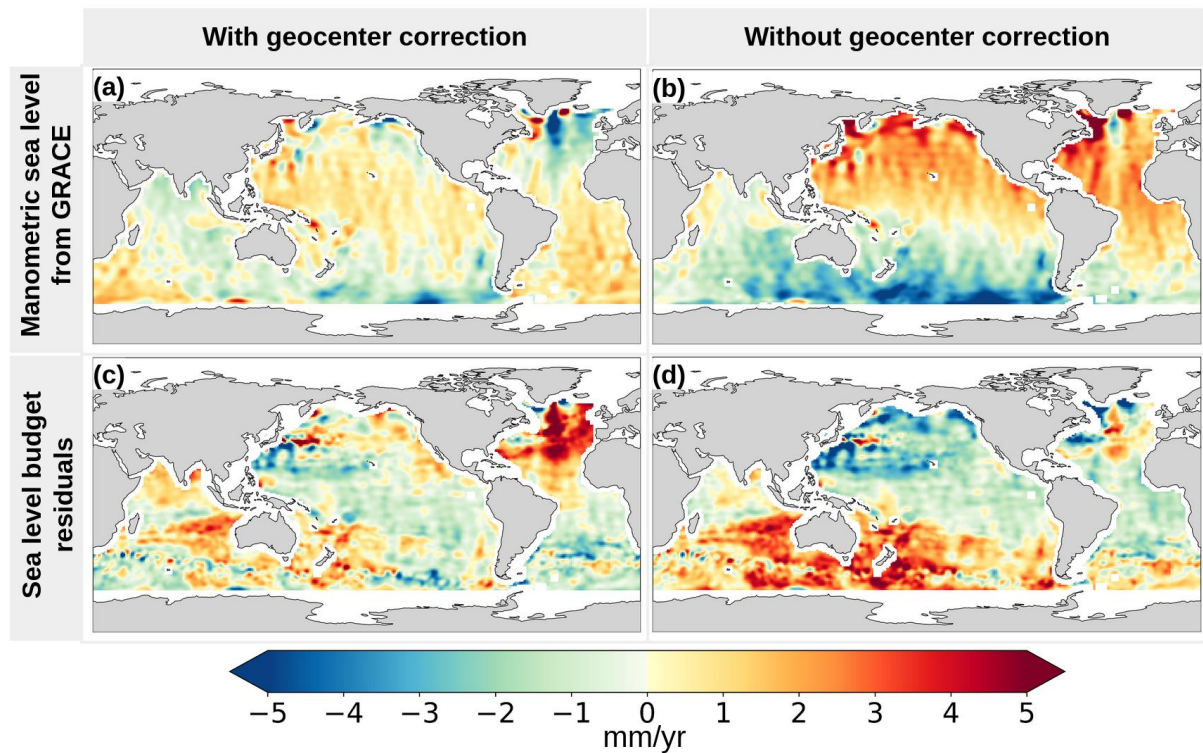
Figure 23: Sea level trends of GRACE-based manometric component and corresponding budget residuals with and without the geocenter correction. (a) Manometric sea level trend map with the geocenter correction, (b) Manometric sea level trend map without the geocenter correction, (c) Sea level budget residual trend map computed with the manometric component corrected for the geocenter, (d) Sea level budget residual trend map computed with the manometric component not corrected for the geocenter.

To estimate the impact of the GIA corrections on the manometric component and budget residuals, we further formed two separate subsets of 30 solutions each, for each GIA model (Peltier et al, 2018 and Caron et al., 2018), applying the Sun et al. (2016)'s geocenter correction to each subset. Unlike for the geocenter case, no significant difference was observed.

5. Regional sea level budget using ocean reanalyses for the manometric component

As explained in section 2, according to Gregory et al. (2019) and Camargo et al. (2023), the dynamic ocean mass redistribution due to ocean circulation changes can be estimated from the sterodynamic sea level corrected for local steric changes. Thus, in this study, we apply Camargo et al. (2023)'s approach and use ocean reanalyses to estimate the manometric component, in order to further assess closure of the regional sea level budget.

As detailed above (section 3), six different ocean reanalyses have been considered over their common period from January 2004 to December 2019. However, to compute the ensemble mean reanalysis, we discarded FOAM because of its spurious trends in the South Atlantic and South Indian Ocean. Figure 34 shows the reanalysis-based manometric trend maps over 2004-2019, for each of the six data sets, as well as the ensemble mean based on CIGAR, C-GLORS, GLORYS, ORAS5 and SODA. The manometric components based on the two sets of GRACE solutions, restricted to this study period, are also shown.

No uncertainties are provided with the reanalyses data so that it is not possible to highlight the areas where the signal is significant for the individual cases (Figure 3a-d). This can be done however for the ensemble mean (Figure 3g) where the errors are estimated from the dispersion of the five reanalyses (CIGAR, C-GLORS, GLORYS, ORAS5 and SODA) about the mean.
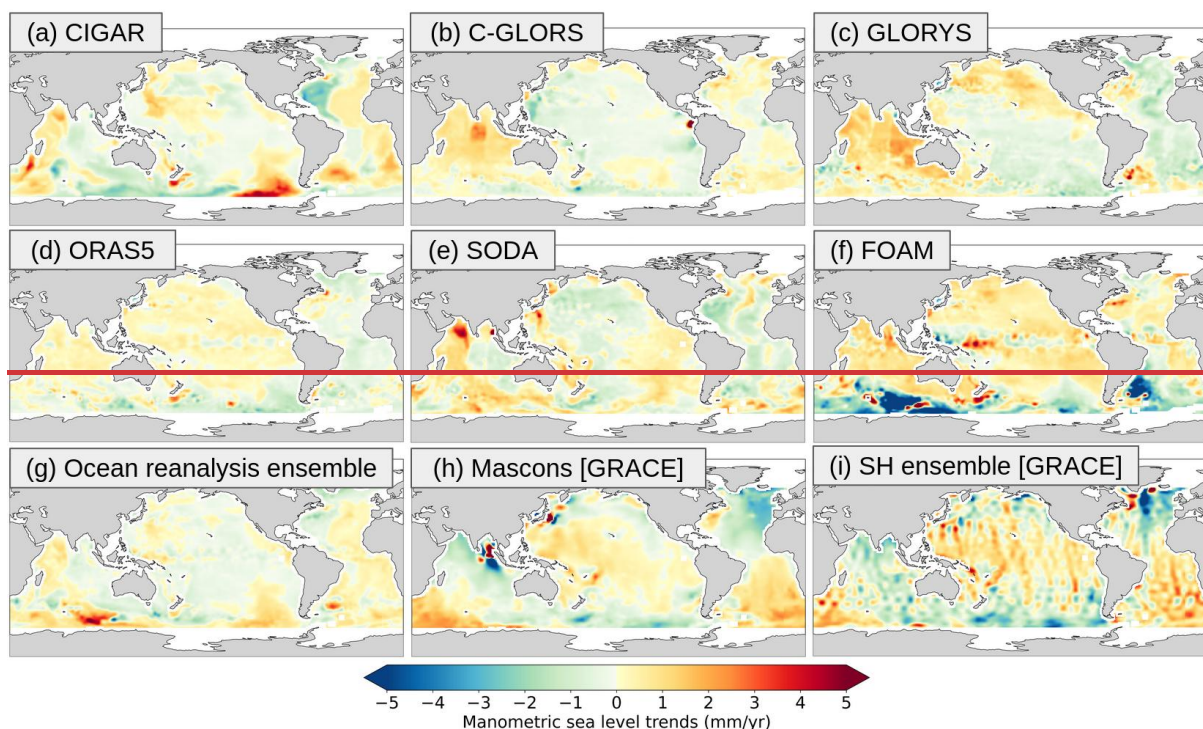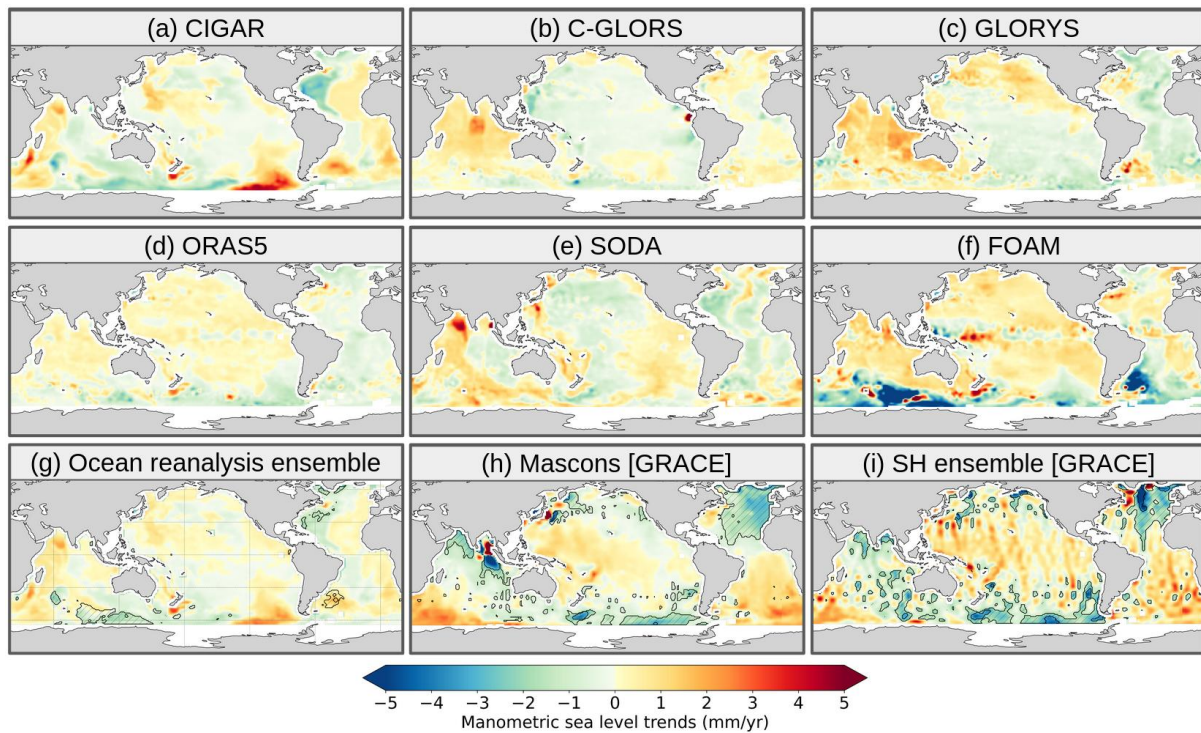
Figure 34: Reanalysis-based manometric trend maps over January 2004-December 2019 for each of the six ocean reanalyses: CIGAR, C-GLORS, GLORYS, ORAS5, SODA and FOAM (panels a to f). Panel (g) shows the ensemble mean of the five reanalyses (CIGAR, C-GLORS, GLORYS, ORAS5 and SODA). Panels h and i refer to the manometric component from the GRACE mascon and GRACE spherical harmonic (SH) ensembles. Hatched areas in panels 3g, 3h, 3i represent regions where the signal is not significant.

The six reanalyses provide quite different manometric trend patterns. The FOAM and ORAS5 patterns are quite similar in the Pacific and Indian Oceans. In these regions, C-GLORS, CIGAR and GLORYS show rough agreement. SODA's patterns differ from the other reanalyses everywhere, although they look similar to CIGAR in the Indian Ocean. As mentioned above, the FOAM-based manometric map shows spurious high trends in the South Atlantic and South Indian Ocean. This is why it is not included in the ensemble mean.

Comparing ensemble mean reanalyses-based manometric map with the GRACE-based manometric maps, we note that : (1) the spatial patterns of the reanalysis-based manometric trend map have generally slightly generally lower amplitude than the GRACE ones in many regions, except around Antarctica. and (2) the manometric spatial trends of the ensemble mean reanalyses and GRACE have opposite signs in many regions, including in the North Atlantic.

504 The regional budget has been computed with each of the six reanalyses as well as for

505 ensemble mean (FOAM excluded), all other data being kept unchanged. The

506 corresponding residual trend patterns are shown in Figure 4<s>5</s>.

507

508
509

510

511
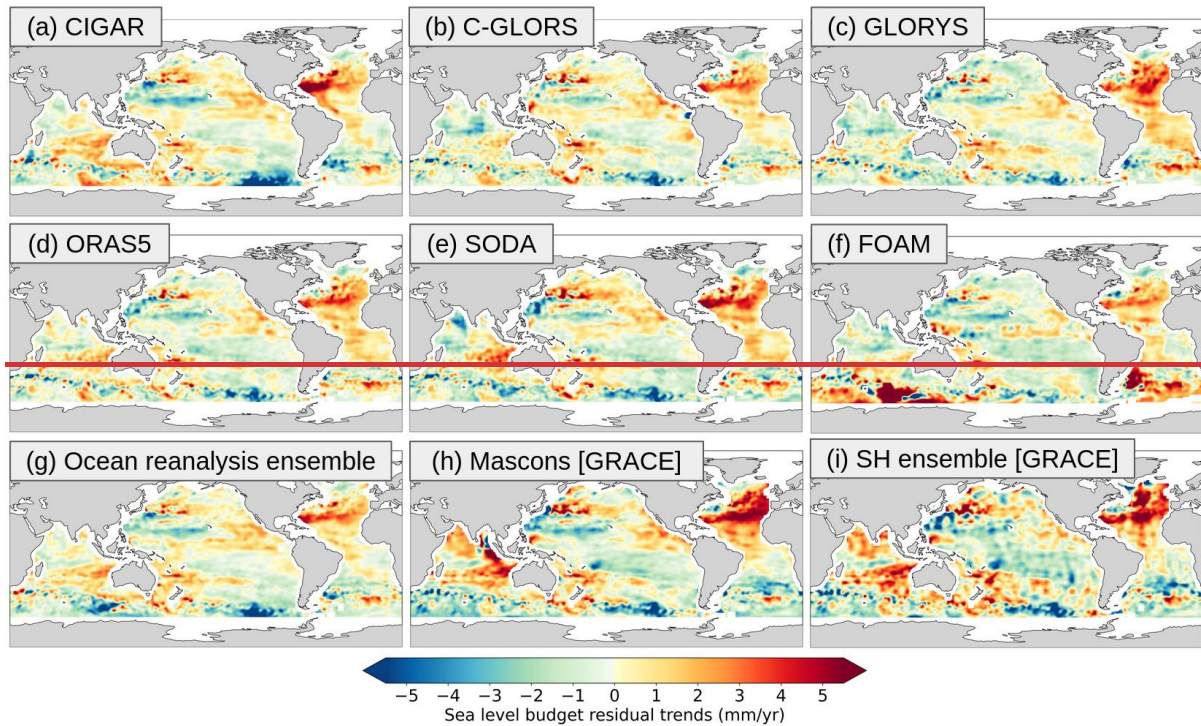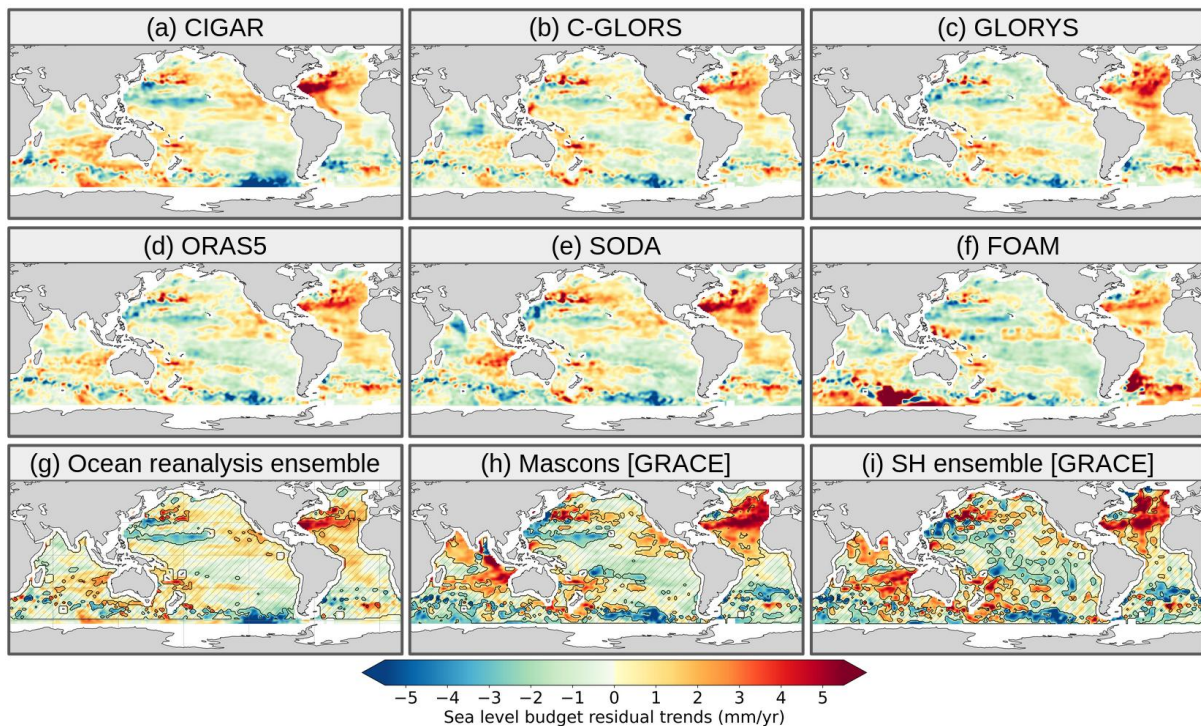
Figure 45: Residual trends of the regional sea level budget computed with each of the six six reanalyses-based manometric componentdata sets, as well as with the ensemble if mean (FOAM excluded) (panels a to g) (with altimetry-based and steric components unchanged). GRACE-based residual trends for both mascons and spherical harmonic solutions are also shown (panels h and i). The period of analysis here is from January 2004 to December 2019. Hatched areas in panels 4g, 4h, 4i represent regions where the signal is not significant.

The CIGAR, C-GLORS, SODA, ORAS5, and GLORYS reanalyses give very similar residual trend patterns, even though SODA uses completely different ocean model and data assimilation schemes, and no altimetry-based sea level data are assimilated. Note that CIGAR also does not assimilate altimetry-based sea level anomaly data, but it is forced by the latest atmospheric reanalysis from ECMWF (unlike the other reanalyses) and embeds a daily varying runoff dataset for freshwater discharge into the oceans. Again, oOne outlier is FOAM which shows strong positive residual trends in the Ssouthern Atlantic and South Indian Oceans. The ensemble mean residual trend map (FOAM excluded) displays a slightly lower signal than the GRACE cases (compare panels 4g with panels 4h and 4i in of Figure 45). What is striking is that the two approaches (reanalyses and GRACE) show positive residual trends in the North Atlantic. However, the residuals are significantly stronger using GRACE, especially in the northeastern part of the Atlantic Ocean. This will be discussed in section 6.

535 Table 2 shows the root mean square (RMS) of the gridded residuals trends over 2004-
536 2019, averaged over the Pacific, Indian, North and South Atlantic Oceans for the
537 reanalyses and GRACE cases.

538 If we exclude except FOAM which displays higher RMS in the Indian and South
539 Atlantic oceans than other reanalyses, Table 2 clearly shows systematically higher
540 RMS (in the range 2-3 mm/yr) in the North Atlantic Ocean for the C-GLORS, SODA,
541 GLORYS and ORAS5 reanalyses as well as for GRACE mascons.

542 Table 2: RMS of gridded residuals trends over 2004-2019, averaged over the Pacific,
543 Indian, North and South Atlantic oceans for the six GRACE and reanalyses and
544 GRACE mascons cases.

545

RMS (mm/yr)	Pacific Ocean	Indian Ocean	North Atlantic Ocean	South Atlantic Ocean
C-GLORS	1.48	1.46	2.02	1.35
FOAM	1.66	2.81	1.99	2.54
SODA	1.58	1.79	2.68	1.56
GLORYS	1.34	1.61	2.49	1.72
ORAS5	1.39	1.38	2.15	1.37
CIGAR	1.51	1.51	2.47	1.46
GRACE mascons	1.51	1.78	2.92	1.43

546

Because four of the reanalyses used above assimilate altimetry data (i.e., C-GLORS, GLORYS, ORAS5 and FOAM), our approach may introduce some circularity to the regional sea level budget assessment. This is the reason for also using reanalyses without altimetry data assimilation (SODA and CIGAR). Here we focus on CIGAR and extend the study period to December 2022. Comparing the manometric components of two reanalyses versions with and without altimetry data assimilation (e.g., C-GLORS and CIGAR, noting however that they differ in terms of resolution, configuration and forcing; Figure 4) shows some differences locally, in particular in the northwestern Atlantic and North Indian Oceans. However, the residual trend maps are very similar. In Figure 5 are shown manometric and residual trend maps based on CIGAR, GRACE mascons and GRACE SH ensemble, extended until 2022. Overall, the patterns are qualitatively similar to those of the shorter period 2004-2019 (Figures 3 and 4). Thus, aAdding three more years does not change the previous conclusion, i.e., that significant residual trends are observed in the North Atlantic (and around Antarctica as well). But the residual patterns in the North Atlantic are noticeably different between CIGAR and GRACE, the maximum signal being located in the western part of the basin for CIGAR and in the eastern part for GRACE.

One may wonder whether the salinity drift observed in some Argo floats as of 2015 has impacted the CIGAR reanalysis since, unlike for altimetry data, T/S data are assimilated during the reanalysis integration, thus non-linearly interacting with dynamical processes computation process. In the reanalysis, the treatment of the salinity drift simply consisted in rejecting data that Argo had flagged for rejection in the delayed mode. But this may not fully guarantee that all bad salinity data have been discarded. However, to compute the reanalysis-based manometric component, the local steric contribution has been removed. Thus, any effect of the spurious Argo salinity drift can be considered as minimal.
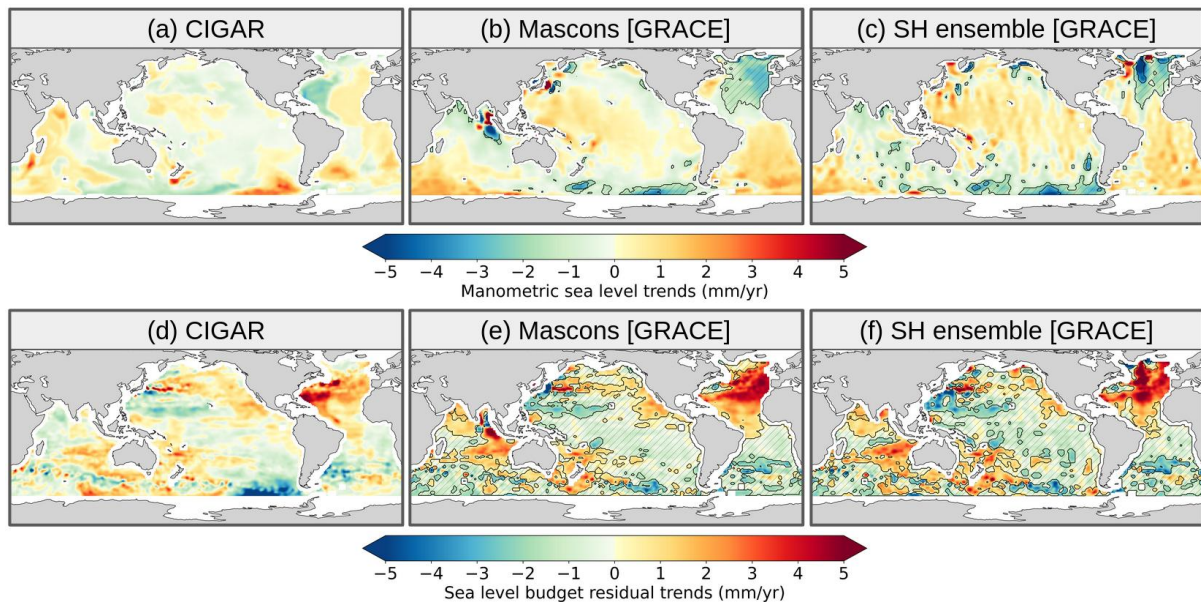
Figure 56: Manometric component based on the CIGAR reanalysis (reanalysis without altimetry data assimilation) (panel a), and the two GRACE solutions (panels b and c). Sea level budget residuals using the CIGAR-based manometric component (panel d) and the two GRACE manometric components (panels e and f). The period of analysis here is from January 2004 to December 2022. Hatched areas in panels 5b,5c, 5e, 5f represent regions where the signal is not significant.

6. Residual trends in the North Atlantic Ocean

In this section, we focus on the North Atlantic Ocean where significant positive residuals are observed when using either GRACE or the CIGAR reanalysis for estimating the manometric component.

Figure 67 shows each component of the budget over the North Atlantic Ocean over January 2004-December 2022, including the computed using three manometric component estimates : GRACE mascons, ensemble mean GRACE SH and CIGAR reanalysis. Associated residual maps (all components unchanged except the manometric one) are also shown.
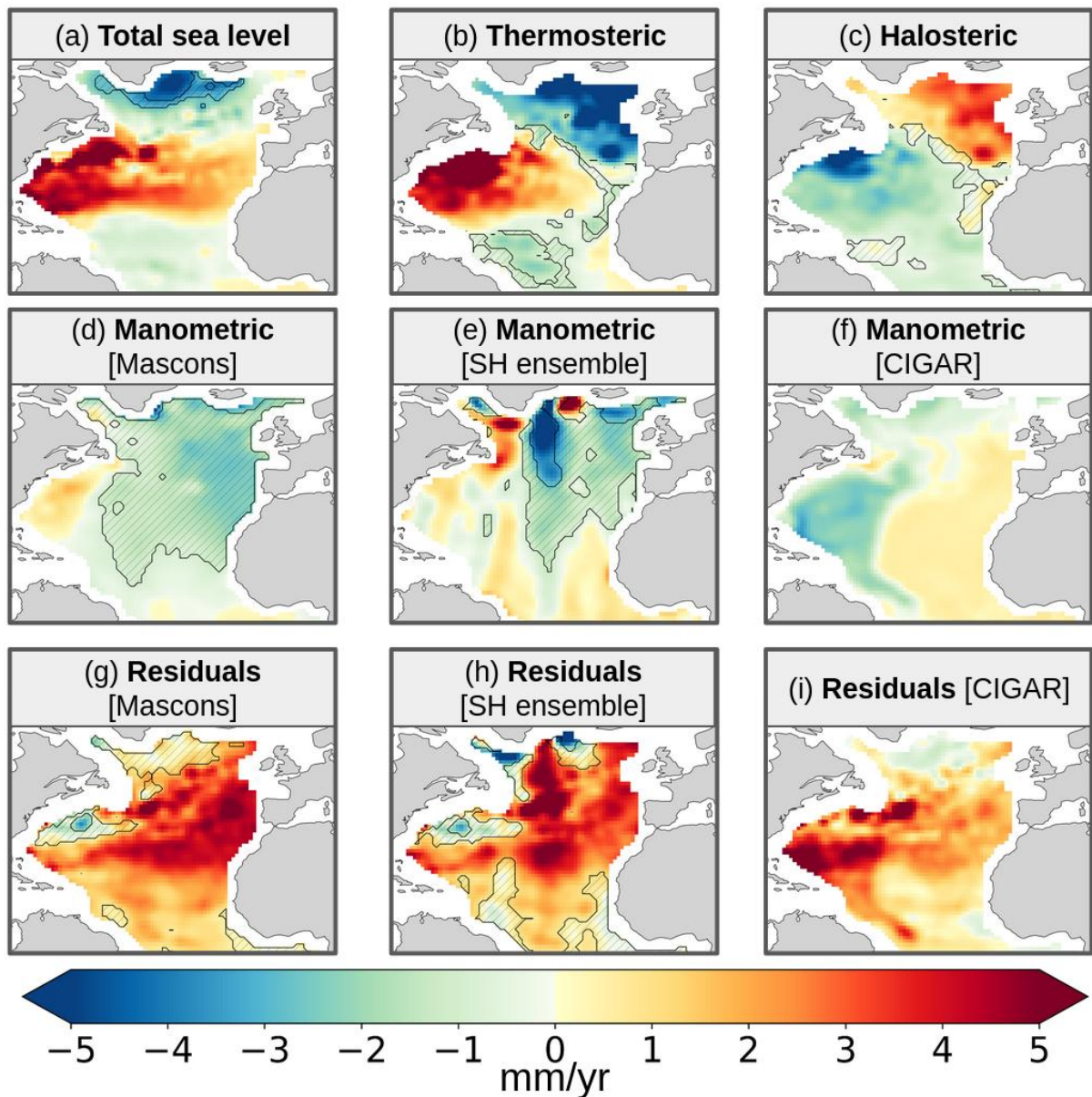
Figure 67: North Atlantic Ocean sea level trends (mm/yr) over January 2004 to December 2022: Observed altimetry-based sea level (a), Argo-based thermosteric and halosteric components (b,c), manometric components from GRACE mascons (d), ensemble mean GRACE spherical harmonics (e) and derived from CIGAR reanalysis (f). Sea level budget residuals (observed sea level trends minus sum of component trends) using GRACE mascons (g), ensemble mean GRACE spherical harmonics (h) and CIGAR (i). Hatched areas represent regions where the signal is not significant.

The North Atlantic Ocean residuals of all three manometric component cases (GRACE mascons, ensemble mean GRACE spherical harmonics and CIGAR) show a positive signal. However, the patterns are significantly different between the reanalysis and GRACE cases. They are localized in the western part of the tropical North Atlantic Ocean with the CIGAR

610 reanalysis and in the eastern part (between the Gibraltar Strait and the Gascogne Gulf) with

611 GRACE mascons. The residuals based on the ensemble mean GRACE spherical harmonics

612 display a strong north-south signal in the mid North Atlantic, likely due to north-south stripe

613 noise affecting spherical harmonic solutions (Blazquez et al., 2018).

614 To further investigate the North Atlantic sea level misclosure, we computed the North Atlantic

615 sea level budget after geographically averaging each component over the region, using

616 GRACE mascons for the manometric component. This is shown in Figure 78, along with the

617 sea level budget, averaging the data globally but excluding the North Atlantic Ocean.

618

619
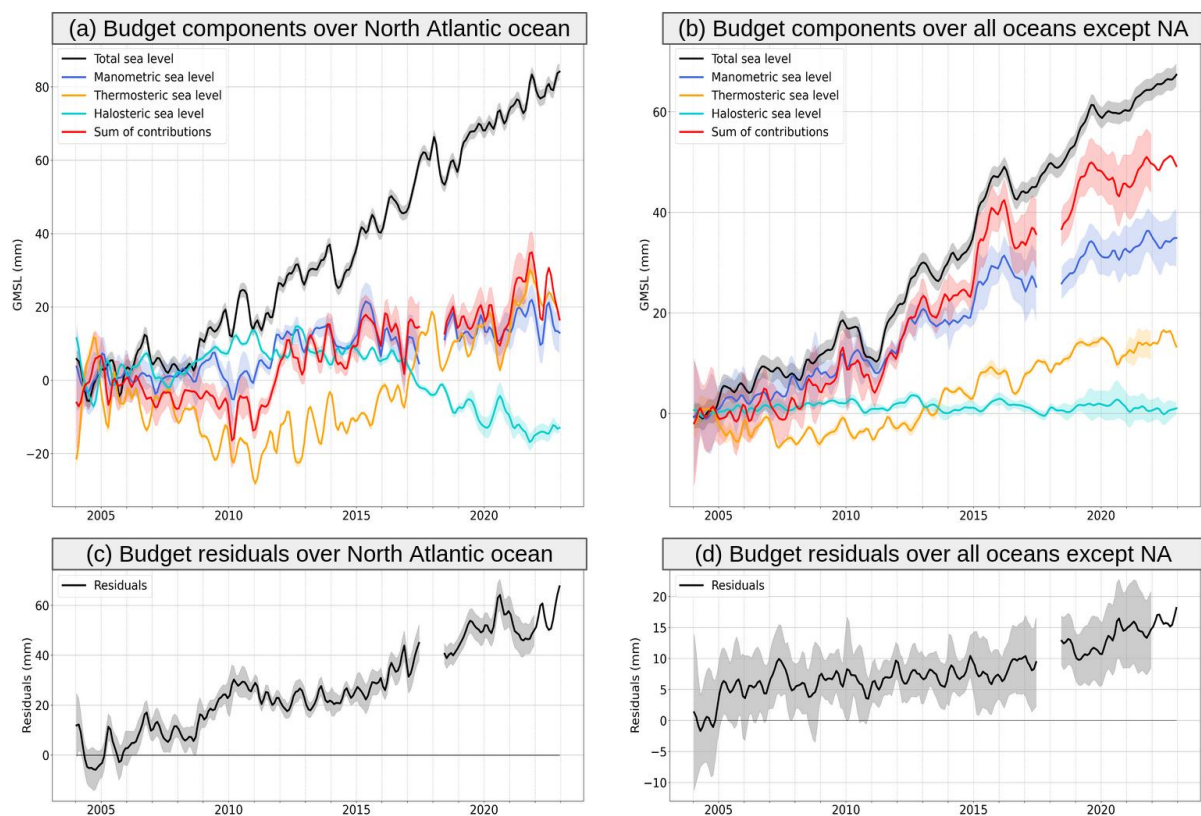
Figure 78: Regionally averaged sea level budget for January 2004 to December 2022, over
the North Atlantic Ocean (a) and over all oceans except the North Atlantic (NA) one (b). On
each panel are shown the altimetry-based sea level (black curve), the thermosteric and
halosteric components (orange and turquoise curves), the manometric component (GRACE
mascons, blue curve) and the sum of all components (red curve). The panels c and d show
the corresponding residuals (observed sea level minus sum of components). Shaded areas
represent the standard one-sigma uncertainties.

627 Figure 78 well confirms the non-closure of the budget over the North Atlantic Ocean, with a

628 significant positive residual trend, whereas in the remaining oceanic domain, no significant

629 residual trend is noticed. Figure 78 (panel a) suggests that the North Atlantic residual trend is

630 related to the observed decrease of the halosteric component as of 2015~~3-2014~~. A similar
631 finding is provided in Mu et al. (2024).
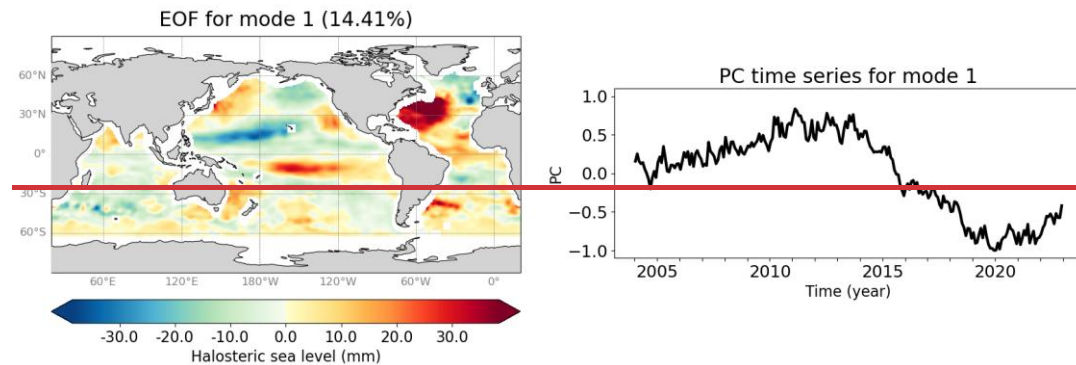
632

638 In order to check whether the North Atlantic residual signal better fits a trend over the study
639 period rather than ~~or~~ a low frequency oscillation, w~~W~~e performed an EOF decomposition over
640 2004-2022 of the gridded residual time series (considering the GRACE SH solution for the
641 manometric component) (see Figure S3 in the Supplementary Information, showing the first
642 two EOF modes). Mode 1 is dominated by a strong residual trend in the North Atlantic. Its
643 spatial map is very similar to the residual map. Mode 2 shows an oscillation of period ~11
644 years on which are ~~is~~ superimposed shorter fluctuations related to ENSO. This EOF
645 decomposition of the residuals confirms the dominant trend contribution of the North Atlantic
646 over the study period.

647

7. Conclusion

649 In this study, we have revisited the regional sea level budget over the GRACE and Argo era.
650 Using different data sets for the manometric component (GRACE and ocean reanalyses), we
651 found significant non-closure of the budget in the North Atlantic Ocean in all studied cases.
652 However, the residual patterns are not localized over the same areas in the GRACE and ocean
653 reanalyses cases. They are stronger in the northeast Atlantic Ocean when considering the
654 GRACE manometric component (mascon solution) while they are more localized in the
655 northwestern tropical part with the reanalysis-based manometric component. The sea level

budget averaged over the whole North Atlantic Ocean leads us to suspect the steric contribution, especially the halosteric component as the main contributor to the budget non-closure in this region, considering that the global budget without the North Atlantic region is closed within the error bars. Although we chose the SIO data set to estimate the steric component, considering that the salinity data had been corrected for the Argo floats instrumental drift that led to spurious salinity measurements, our study points to remaining errors affecting the halosteric component, especially as of 2015. Mu et al. (2024) also reportsuggest a potential salinity bias in the Argo data set of the North Atlantic. Our results suggest that the salinity adjustment to the WOCE salinity climatology proposed by the SIO methodology may not fully correct for the rapid salinity drift experienced by some Argo floats. However, the different locations of the North Atlantic residual patterns when considering the reanalyses or GRACE for the manometric component, as well as larger residuals in the northeast Atlantic Ocean in the GRACE case, suggest that uncertainty in GRACE data also plays a role. In other oceanic regions, a few areas display some small-scale residual structures (e.g., in the north and eastern Pacific and northwest Indian Ocean). This may eventually result from differences in resolution of the gridded data sets used in this study (e.g., satellite altimetry better resolves small scale features than GRACE or Argo), even though the same a low pass filter was applied to all data sets. .

The problem of the North Atlantic halosteric component highlighted in our regional budget study needs to be fixed up at the processing level of the Argo-based measurements. Our findings are helpful to the scientific groups involved in the Argo network as we can identify regions where the salinity contribution to regional sea level change appears to be spurious. This may help them in refining their investigations on the quality control checks to be applied to the Argo profiles. In addition, detailed investigation of the GRACE contribution to the residuals of this region should also be carried out in parallel. Our study highlights the necessity of applying consistent data processing and using similar reference systems for satellite altimetry and gravimetry data. Improved data should indeed be made available to the community, not only for sea level budget assessments but also for other applications in oceanography or climate-related research (i.e., for Earth's energy imbalance studies based on sea level budget approaches).

Acknowledgements

We thank two anonymous reviewers for their helpful comments. We also thank the Magellium/LEGOS climate change team for providing us with the ensemble mean of the GRACE-based spherical harmonics solutions and for fruitful discussions.

This research was carried out under a programme of, and funded by, the European Space Agency (ESA) Climate Change Initiative, within the project entitled "Sea level budget closure CCI+ (SLBC_CCI+)" (contract number 4000140620/23/I-BN). Part of this work is a contribution to the GREAT project which is supported by the Centre National d'Etudes Spatiales (CNES) through the Ocean Surface Topography Science Team (OSTST).

Part of this work was also performed in the context of the ERC Synergy GRACEFUL project (ERC Synergy grant n° 855677).

Authors contribution

Conceptualization: MB, AB (Barnoud), AC. Data analysis: MB, AB (Barnoud). Reanalysis computation: CY, AS. Writing original draft: AC. Final writing, review and editing: all co-authors.

Conflict of interest

The authors declare no conflict of interest relevant to this study.

References

Ablain M., R. Jugier, L. Zawadki, and N. Taburet (2017). "The TOPEX-A Drift and Impacts on GMSL Time Series." AVISO Website. October 2017. https://meetings.aviso.altimetry.fr/fileadmin/user_upload/tx_ausyclsseminar/files/Poster_OST ST17_GMSL_Drift_TOPEX-A.pdf.

Ablain, M., Meyssignac B., Zawadski, L., Jugler R., Ribes, A., Spada, G., Benveniste, J., Cazenave, A. and Picot, N. (2019), Uncertainty in satellite estimates of global mean sea-level changes, trend and acceleration, *Earth Syst. Sci. Data*, 11, 1189–1202.

Adhikari, S., Ivins, E. R., Frederikse, T., Landerer, F. W., and Caron, L. (2019). Sea-level fingerprints emergent from GRACE mission 573 data, *Earth Syst. Sci. Data*, 11, 629–646, https://doi.org/10.5194/essd-11-629-2019.

Barnoud, A., Pfeffer, J., Cazenave, A., Fraudeau, R., Rousseau, V., & Ablain, M. (2023). Revisiting the global mean ocean mass budget over 2005–2020. *Ocean Science*, 19, 321–334, https://doi.org/10.5194/os-19-321-2023.

Barnoud A. et al. (2021). Contributions of altimetry and Argo to non-closure of the global mean sea level budget since 2016, published online 26 June 2021, *Geophys. Res. Lett.*, https://doi.org/10.1029/2021GL092824.

Blazquez A., Meyssignac B., Lemoine J.M., Berthier E., Ribes A. and Cazenave A. (2018). Exploring the uncertainty in GRACE estimates of the mass redistributions at the Earth' surface. Implications for the global water and sea level budgets, *Geophysical Journal International*, 215(1), 415-430.

Blockley, E. W., Martin, M. J., McLaren, A. J., Ryan, A. G., Waters, J., Lea, D. J., Mirouze, I., Peterson, K. A., Sellar, A., and Storkey, D. (2014). Recent development of the Met Office operational ocean forecasting system: an overview and assessment of the new Global FOAM forecasts, *Geosci. Model Dev.*, 7, 2613–2638, https://doi.org/10.5194/gmd-7-2613-2014.

Brown S, Willis J, Fournier S. (2023). Jason-3 wet path delay correction. Ver. F. PO.DAAC, CA, USA. https://doi.org/10.5067/J3L2G-PDCOR.

Camargo C.M. et al. (2023). Regionalizing the sea level budget with machine learning techniques, *Ocean Science*, 19, 17-41, https://doi.org/10.5194/os-19-17-2023.

Caron, L., Ivins, E. R., Larour, E., Adhikari, S., Nilsson, J., & Blewitt, G. (2018). GIA model statistics for GRACE hydrology, cryosphere and ocean science. *Geophysical Research Letters*, 45, 2203– 2212. https://doi.org/10.1002/2017GL07664.

Carrere L. and Lyard F. (2003), Modeling the barotropic response of the global ocean to atmospheric wind and pressure forcing. Comparisons with observations. *Geophys. Res. Lett.* 30, 6, 1275, https://doi.org/10.1029/2002GL016473.

Carret, A., Llovel, W., Penduff, T., & Molines, J.-M. (2021). Atmospherically forced and chaotic interannual variability of regional sea level and its components over 1993–2015. *Journal of Geophysical Research: Oceans*, 126, e2020JC017123. ~~https://doi.org/10.1029/2020JC017123~~https://doi.org/10.1029/2020JC017123

Carret A., Johannessen J., Andersen O., Ablain M., Prandi P., Blazquez A. and Cazenave A. (2017). Arctic sea level during the altimetry era, *Surveys in Geophysics*, 38, 251-277, https://doi.org/10.1007/s10712-016-9390-2.

Carton, J. A., G. A. Chepurin, and L. Chen (2018). SODA3: A New Ocean Climate Reanalysis. *J. Climate*, 31, 6967–6983, https://doi.org/10.1175/JCLI-D-18-0149.1.

Cazenave A., Palanisamy H. and Ablain M. (2018). Contemporary sea level changes from satellite altimetry: What have we learned? What are the new challenges? *Advances in Space Research*, https://doi.org/10.1016/j.asr.2018.07.017, published online 27 July 2018.

Cazenave A. and Moreira L. (2022). Contemporary sea level changes from global to local scales: a review, *Proc. Royal Society*, 478, 20220049. https://doi.org/10.1098/rspa.2022.0049.

Chen, J.L., Tapley, B. D., Save, H., Tamisiea, M. E., Bettadpur, S., & Ries, J. (2018). Quantification of ocean mass change using gravity recovery and climate experiment, satellite altimeter, and Argo floats observations. *Journal of Geophysical Research: Solid Earth*, 123, 10,212–10,225. https://doi.org/10.1029/2018JB016095.

Chen J.L., Tapley B.D., Seo K-W., Wilson C. and Ries J. (2019), Improved Quantification of Global Mean Ocean Mass Change Using GRACE Satellite Gravimetry Measurements ». *Geophysical Research Letters* 46, 23, 13984-91. https://doi.org/10.1029/2019GL085519.

Chen J.L., Tapley B.D., Wilson C., Cazenave A., Seo K-W and Kim J.S. (2020). Global ocean mass change from GRACE 1 and GRACE Follow-On, and altimeter and Argo measurements,

Geophys. Res. Lett., https://doi.org/10.1029/2020GL090656, published online, 3 November 2020.

Dangendorf S, Frederikse T, Chafik L, Klinck JM, Ezer T, Hamlington BD. (2021). Data-driven reconstruction reveals large-scale ocean circulation control on coastal sea level. *Nat. Clim.Change* 11, 514–520. https://doi.org/10.1038/s41558-021-01046-1.

Dieng H.B., Cazenave A., Meyssignac B. and Ablain M. (2017). New estimate of the current rate of sea level rise from a sea level budget approach, *Geophys. Res. Lett.*, 44, https://doi/org/10.1002/2017GL073308.

Dobslaw, H., Bergmann-Wolf, I., Dill, R., Poropat, L., Thomas, M., Dahle, C., et al. (2017). A new high-resolution model of non-tidal atmosphere and ocean mass variability for de-aliasing of satellite gravity observations: AOD1B RL06. *Geophysical Journal International*, 211(1), 263-269, https://doi.org/10.1093/gji/ggx302.

England, M.H., McGregor, S., Spence, P., Meehl, G. A. (2014). Recent intensification of wind-driven circulation in the Pacific and the ongoing warming hiatus. *Nature Climate Change*, **4**, 222-227, https://doi.org/10.1038/NCLIMATE2106.

Flechtner, F., Dobslaw, H. & Fagiolini, E. (2015). AOD1B Product Descrip tion Document for Product Release 05 Rev4.4 GRACE 327–750, Geo Forschungszentrum Potsdam, Potsdam, Germany.

Forget, G., and Ponte, R. M. (2015). The partition of regional sea level variability. *Progr. Oceanogr*. 137, 173–195. https://doi.org/10.1016/j.pocean.2015.06.002.

Frederikse, T., Riva, R., Kleinherenbrink, M., Wada, Y., den Broeke, M. van, and Marzeion, B. (2016), Closing the sea level budget on a regional scale: Trends and variability on the Northwestern European continental shelf, *Geophys. Res. Lett.*, 43, 10,864– 10,872, https://doi.org/10.1002/2016GL070750.

Frederikse, T., Jevrejeva, S., Riva, R. E. M., & Dangendorf, S. (2018). A Consistent Sea-Level Reconstruction and Its Budget on Basin and Global Scales over 1958–2014, *Journal of Climate*, 31(3), 1267-1280, https://journals.ametsoc.org/view/journals/clim/31/3/jcli-d-17-0502.1.xml.

Frederikse T et al. (2020). The causes of sea-level rise since 1900. *Nature* 584, 393–397, https://doi.org/10.1038/s41586-020-2591-3.

Garric, G., and Parent, L. (2017). Quality Information Document for Global 1330 Ocean Reanalysis Products Global-Reanalysis-Phy-001-025. Available online at: https://catalogue.marine.copernicus.eu/documents/QUID/CMEMS-GLO-QUID-001-025.pdf

Gregory, J. M. & Lowe, J. A. (2000). Predictions of global and regional sea-level rise using AOGCMs with and without flux adjustment. *Geophysical Research Letters*, 27(19), 3069-3072. https://doi.org/10.1029/1999GL011228.

Gregory J.M. et al. (2019). Concepts and Terminology for Sea Level: Mean, Variability and Change, Both Local and Global, *Surveys in Geophysics*, 40:1251–1289, https://doi.org/10.1007/s10712-019-09525-z.

Good, S. A., M. J. Martin and N. A. Rayner (2013). EN4: quality controlled ocean temperature and salinity profiles and monthly objective analyses with uncertainty estimates, *Journal of Geophysical Research: Oceans*, 118, 6704-6716, https://doi;org/10.1002/2013JC009067.

808 Guérou, A., Meyssignac, B., Prandi, P., Ablain, M., Ribes, A., and Bignalet-Cazalet, F. (2023).
809 Current observed global mean sea level rise and acceleration estimated from satellite altimetry
810 and the associated measurement uncertainty, *Ocean Sci.,* 19, 431–451,
811 https://doi.org/10.5194/os-19-431-2023.

812 Hamlington et al. (2020). Undertstanding contemporary regional sea level change and the
813 implications for the future, *Review of Geophysics*, https://doi.org/10.1029/2019RG000672.

814 Hamlington, B. D., Cheon, S. H., Piecuch, C. G., Karnauskas, K. B., Thompson, P. R., Kim,
815 K.-Y., et al. (2019). The dominant global modes of recent internal sea level variability. *Journal*
816 *of Geophysical Research: Oceans*, 124, 2750–2768. https://doi.org/10.1029/2018JC014635.

817 Han, W., Meehl, G., Stammer, D., Hu, A., Hamlington, B., Kenigson, J., et al. (2017). Spatial
818 patterns of sea level variability associated with natural internal climate modes. *Surveys in*
819 *Geophysics*, 38(1), 217–250. https://doi.org/10.1007/s10712-016-9386-y.

820 Han W., Stammer D., Thompson P., Ezer T., Palanisamy H., Zhang X., Domingues C., Zhang
821 L., Yuan D., (2019). Impacts of Basin-Scale Climate Modes on Coastal Sea Level: a Review,
822 *Surveys in Geophysics*, 40, 1493–1541, https://doi.org/10.1007/s10712-019-09562-8.

823 Horwath M., Gutknecht B., Cazenave A., et al., (2022). Global sea level budget and ocean
824 mass budget, with focus on advanced data products and uncertainty characterization. *Earth*
825 *System Science Data*, 14, 411–447, 2022 https://doi.org/10.5194/essd-14-411-2022.

826 IPCC (2019). IPCC Special Report on the Ocean and Cryosphere in a Changing Climate,
827 edited by Portner, H.-O., Roberts, D. C., Masson-Delmotte, V., Zhai, P., Tignor, M.,
828 Poloczanska, E., Mintenbeck, K., Alegriìa, A., Nicolai, M., Okem, A., Petzold, J., Rama, B.,
829 and Weyer, N. M.

830 IPCC (2021), Climate Change 2021. The Physical Science Basis. Contribution of Working
831 Group I to the Sixth Assessment Report of the Intergovernmental Panel on Climate Change
832 [Masson-Delmotte, V., P. Zhai, A. Pirani, S.L. Connors, C. Péan, S. Berger, N. Caud, Y. Chen,
833 L. Goldfarb, M.I. Gomis, M. Huang, K. Leitzell, E. Lonnoy, J.B.R. Matthews, T.K. Maycock, T.
834 Waterfield, O. Yelekçi, R. Yu, and B. Zhou (eds.)]. Cambridge University Press. In Press.

835 Llovel, W., and T. Lee (2015), Importance and origin of halosteric contribution to sea level
836 change in the southeast Indian Ocean during 2005–2013, *Geophys. Res. Lett.*, 42, 1148–
837 1157, https://doi.org/10.1002/2014GL062611.

838 Llovel, W., Balem, K., Tajouri, S., & Hochet, A. (2023). Cause of substantial global mean sea
839 level rise over 2014–2016. *Geophysical Research Letters*, 50, e2023GL104709.
840 https://doi.org/10.1029/2023GL104709.

841 Loomis, B. D., Luthcke, S. B., & Sabaka, T. J. (2019). Regularization and error characterization
842 of GRACE mascons. *Journal of Geodesy*, 93(9), 1381–1398. https://doi.org/10.1007/s00190-
843 019-01252-y.

844 Lorbacher, K., Marsland, S. J., Church, J. A., Griffies, S. M., Stammer, D. (2012). Rapid
845 barotropic sea level rise from ice sheet melting. *Journal of Geophysical Research*, 117,
846 C06003, https://doi.org/10.1029/2011JC007733.

847 Liu C., Liang X., Ponte R.M.. and Chambers D.P. (2020). Global patterns of spatial and
848 temporal variability in multiple gridded salinity products, *J. Climate*, 33, 20, 8751-8766,
849 https://doi.org/10.1175/jcli-d-20-0053.1.

850 Liu C., Liang X., Ponte R.M. and Chambers D.P. (2024). 3Salty Drifts" of argo floats affects
851 the gridded ocean salinity products, *J. Geophys. Res. -Oceans*, 129, c2023JC020871,
852 https://doi.org/10.1019/2023JC020871.

853 Ludwigsen C.B. et al. (2024). Global and regional ocean mass budget closure since 2003,
854 *Nature Communications,* 15, 1416, https://doi.org/10.1038/s41467-024-45726-w.

855 Ludwigsen C.B., Andersen O.B. and rose S.K. (2022), Components of 20 years (1995-2015)
856 of absolute sea level trends in the Arctic, *Ocean Science*, 181,109-127,
857 https://doi.org/10.5194/os-18-109-2022.

858 Merrifield, M. A., and Maltrud, M. E. (2011), Regional sea level trends due to a Pacific trade
859 wind intensification, *Geophys. Res. Lett.*, 38, L21605, https://doi.org/10.1029/2011GL049576.

860 Milne G.A., Gehrels W.R., Hughes C.W. and Tamisea M.E. (2009), Identifying the causes of
861 sea level change, *Nature Geosci* 2, 471–478. https://doi.org/10.1038/ngeo544.

862 Mitrovica J, Tamisiea ME, Davis JL, Milne GA. (2001). Recent mass balance of polar ice
863 sheets inferred from patterns of global sea-level change. *Nature,* 409, 1026–1029,
864 https://doi.org/10.1038/35059054.

865 Mu D., Church J.A., King M., Ludwigsen C.B. and Xu T. (2024). Contrasting discrepancy in
866 the sea level budget between the North and South Atlantic Ocean since 2016, *Earth and
867 Space Science,* 11, e2023EA003133, https://doi.org/10.1029/2023EA003133.

868 Nerem, R.S., Beckley, B.D., Fasullo, J., Hamlington, B.D., Masters, D. and Mitchum, G.T.
869 (2018). Climate Change Driven Accelerated Sea Level Rise Detected In The Altimeter Era,
870 *Proceedings of the National Academy of Sciences,* 15, 9, 2022-2025,
871 https://doi.org/10.1073/pnas.1717312115.

872 Peltier R.W. (2004), Global Glacial Isostasy and the Surface of the Ice-Age Earth: The ICE-
873 5G (VM2) Model and GRACE, *Annual Review of Earth and Planetary Science*, 32, 111-149.

874 Peltier R.W., D. F. Argus, and R. Drummond (2018). "Comment on "An assessment of the
875 ICE-6G_C (VM5a) glacial isostatic adjustment model" by Purcell et al." *Journal of Geophysical
876 Research- Solid Earth* 123, 2, 2019-2028.

877 Piecuch CG and Ponte RM. (2014). Mechanisms of global mean steric sea level change. *J.
878 Clim.* 27, 824–834, https://doi.org/10.1175/JCLI-D-13-00373.1.

879 Ponte R.M., Sun Q., Liu C. and Liang X. (2021). How salty is the global ocean: weighting it all
880 or tasting it a sip at a time, *Geophys. Res. Lett.*, 48, 11, e2021GL092935,
881 https://doi.org/10.1029/2021gl092935.

882 Prandi, P., Meyssignac, B., Ablain, M. et al. (2021). Local sea level trends, accelerations and
883 uncertainties over 1993–2019. *Nature Sci Data*, 626, 8, 1. https://doi.org/10.1038/s41597-020-
884 00786-7.

885 Proshutinsky AIM, Ashik EN, Dvorkin S, Häkkinen RA, Krishfield PWR. (2004). Secular sea
886 level change in the Russian sector of the Arctic Ocean. *J. Geophys. Res.* 109, C03042,
887 https://doi.org/10.1029/2003JC002007.

888 Purkey SG, Johnson GC. (2010). Warming of Global Abyssal and Deep Southern Ocean
889 Waters between the 1990 s and 2000 s, contributions to Global Heat and Sea Level Rise
890 Budgets. *J. Clim.* 23, 6336–6351, https://doi.org/10.1175/2010JCLI3682.1.

891 Rietbroek, R., Brunnabend, S. E., Kusche, J., Schröter, J., and Dahle, C. (2016). Revisiting
892 the contemporary sea-level budget on global and regional scales. *Proc. Natl. Acad. Sci.*, 113,
893 1504–1509. https://doi.org/10.1073/pnas.1519132113.

894 Roberts CD, Calvert D, Dunstone N, Hermanson L, Palmer MD, Smith D. (2016). On the
895 drivers and predictability of seasonal to interannual variations in regional sea level. J. Clim.
896 29, 7565–7583, https://doi.org/10.1175/JCLID-D-15-0886.1.

897 Roemmich D, Gilson J. (2009). The 2004–2008 mean and annual cycle of temperature,
898 salinity, and steric height in the global ocean from the Argo Program. *Prog. Oceanogr.* 82, 81–
899 100, https://doi.org/10.1016/j.pocean.2009.03.004.

900 Royston, S., Vishwakarma, B. D., Westaway, R. M., Rougier, J., Sha, Z., and Bamber, J. L.
901 (2020). Can we resolve the basin-scale sea level 557 trend budget from GRACE ocean mass?
902 *Journal of Geophysical Research- Oceans*, 125, e2019JC015535. 558,
903 https://doi.org/10.1029/2019JC015535.

904 Save H., Bettadpur S. and Tapley B.D. (2016). High resolution CSR GRACE RL05 mascons,
905 *J. Geophys. Res. Solid Earth*, 121, 7547-7569, https://doi.org/10.1002/2016jB013007.

906 Spada, G. (2017). Glacial isostatic adjustment and contemporary sea level rise: An overview.
907 *Surveys in Geophysics*, 38, 153- 587 185. https://doi.org/10.1007/s10712-016-9379-x.

908 Sun, Y., Riva, R., & Ditmar, P. (2016). Optimizing estimates of annual variations and trends in
909 geocenter motion and J2 from a combination of GRACE data and geophysical models. *Journal*
910 *of Geophysical Research,* 121(11), 8352-8370. https://doi.org/10.1002/2016JB013073.

911 Stammer D., Cazenave A., Ponte R. M., Tamisiea M. E. (2013). Causes for contemporary
912 regional sea level changes. *Ann Rev Mar Sci.* 567, 5, 21- 46. https://doi.org/10.1146/annurev-
913 marine-121211-172406.

914 Storto, A. and Masina, S (2016). C-GLORSv5: an improved multipurpose global ocean eddy-
915 permitting physical reanalysis, *Earth Syst. Sci. Data*, 8, 679–696, https://doi.org/10.5194/essd-
916 8-679-2016.

917 Storto, A., Yang, C. (2024). Acceleration of the ocean warming from 1961 to 2022 unveiled by
918 large-ensemble reanalyses. *Nat Commun* 15, 54, https://doi.org/10.1038/s41467-024-44749-
919 7.

920 Storto, A., Chierici, G., Pfeffer, J., Barnoud, A., Bourdalle-Badie, R., Blazquez, A., Cavaliere,
921 D., Lalau, N., Coupry, B., Drevillon, M., Fourest, S., Larnicol, G., and Yang, C. (2024).
922 Variability in manometric sea level from reanalyses and observation-based products over the
923 Arctic and North Atlantic oceans and the Mediterranean Sea, in: 8th edition of the Copernicus
924 Ocean State Report (OSR8), edited by: von Schuckmann, K., Moreira, L., Grégoire, M.,
925 Marcos, M., Staneva, J., Brasseur, P., Garric, G., Lionello, P., Karstensen, J., and
926 Neukermans, G., Copernicus Publications, State Planet, 4-osr8, 12,
927 https://doi.org/10.5194/sp-4-osr8-12-2024.

928 Swenson, S., Chambers, D., & Wahr, J. (2008). Estimating geocenter variations from a
929 combination of GRACE and ocean model output. *Journal of Geophysical Research*, 113, B8410.
930 https://doi.org/10.1029/2007JB005338.

931 Tamisiea, M. E. (2011). Ongoing glacial isostatic contributions to observations of sea level
932 change. *Geophys. J. Int.* 186, 1036–1044. https://doi.org/10.1111/j.1365-246X.2011.05116.x.

933 Tajouri S., W. Llovel, F. Sévellec, J.M. Molines, P. Mathiot, et al. (2024). Simulated Impact of
934 Time-Varying River Runoff and Greenland Freshwater Discharge on Sea Level Variability in
935 the Beaufort Gyre Over 2005–2018. *Journal of Geophysical Research. Oceans*, 129, 9,
936 https://doi.org/10.1029/2024JC021237.

937 Tapley, B., Watkins, M. M., Flechtner, F., Reigber, C. et al. (2019). Contributions of GRACE
938 to understanding climate change, *Nature Climate Change*, 9, 358–369.
939 https://doi.org/10.1038/s41558-019-0456-2.

940 Timmermann, A., McGregor, S., Jin, F. -F. (2010), Wind effects on past and future regional
941 sea level trends in the southern Indo-Pacific. *Journal of Clim*ate, **23**(16), 4429–4437,
942 https://doi.org/10.1175/2010JCLI3519.1.

943 Wang O., Lee T., Piecuch C.G., Fukumori I., Fenty I., Frederiske T. et al. (2022). Local and
944 remote forcing of interannual sea level variability at Nantucket Island, *J. Geophys. Res.
945 Oceans*, 127, 6,e2021JC018275, https://doi.org/10.1029/2021jc018275.

946 Watkins, M. M., Wiese, D. N., Yuan, D.-N., Boening, C., & Landerer, F. W. (2015). Improved
947 methods for observing Earth's time variable mass distribution with GRACE using spherical cap
948 mascons. *Journal of Geophysical Research: Solid Earth,* 120, 2648–2671.
949 https://doi.org/10.1002/2014JB011547.

950 WCRP Global Sea Level Budget Group (The) (2018). Global sea level budget, 1993-present,
951 *Earth System Science Data*, 10, 1551-1590, https://doi.org/10.5194/essd-10-1551-2018.

952 Wong A., Gilson J. and Cabanes C. (2023). Argo salinity: bias and uncertainty evaluation,
953 *Earth Syst. Sci.data*, 15, 383-393, https://doi.org/10.5194/essd-15-383-2023.

954 Wunsch C and Stammer D. (1997). Atmospheric loading and the oceanic 'inverted barometer'
955 effect. *Rev. Geophys.* 35, 79–107, https://doi.org/10.1029/96RG03037.

956 Zuo H., Balmaseda M.A., Tietsche S., Mogensen K., Mayer M. (2019), The ECMWF
957 operational ensemble reanalysis–analysis system for ocean and sea ice: A description of the
958 system and assessment. *Ocean Sci.* 15, 779–808.

Supplementary Information

I. Trend and trend uncertainties ~~errors~~ of altimetry-based sea level, components and budget residuals over 2004-2022

[2]

963
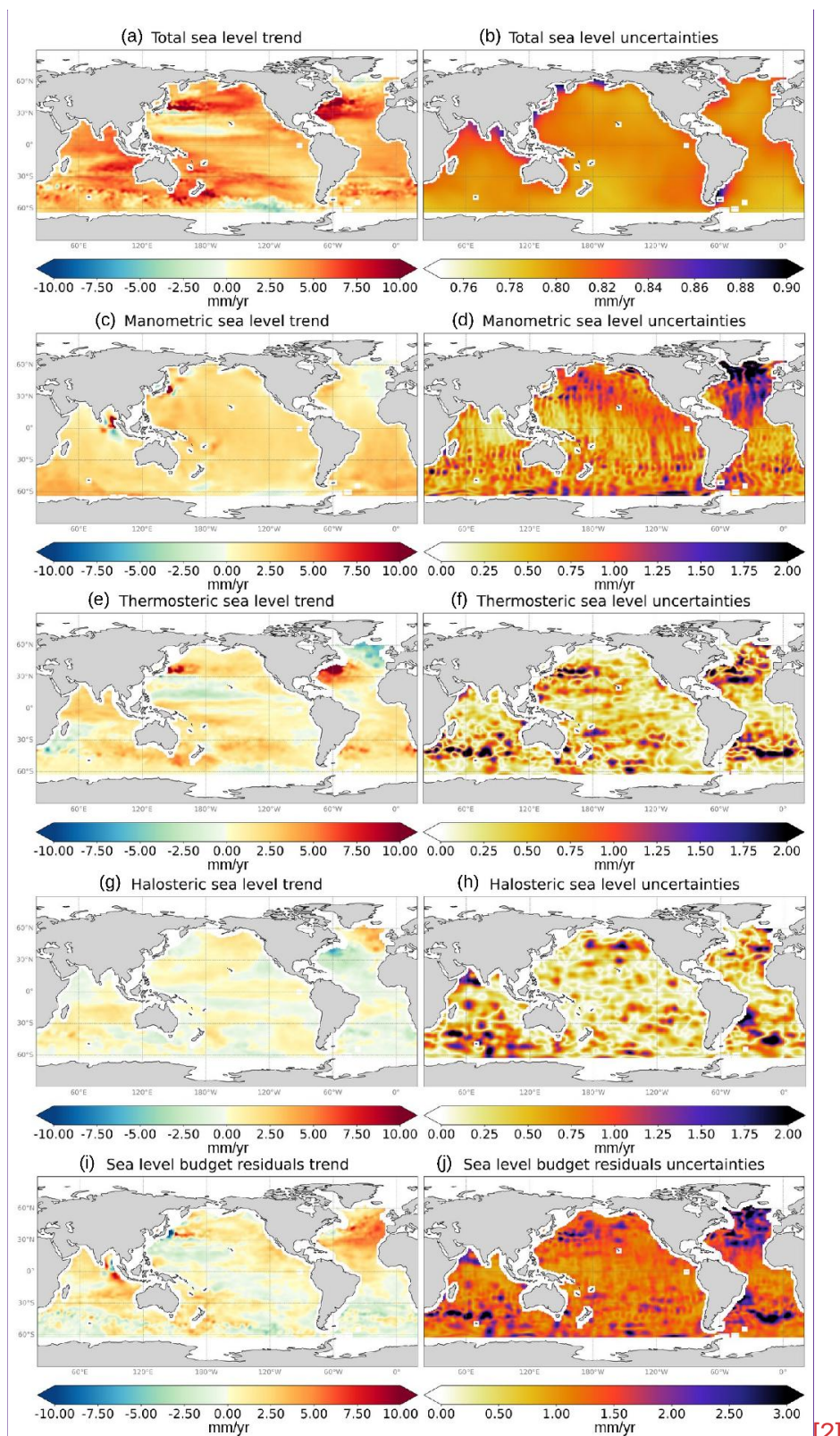
964 *Figure S1: Trend map (left panel) and associated* 1-sigma *trend uncertainty* ~~error~~ *map (right*
965 *panel) over 2004-2022 for each term of the regional sea level budget: (a,b) Total altimetry-*
966 *based sea level trends an*~~ds~~ *associated trend* uncertainties~~errors~~*, (c,d) GRACE-based*
967 *manometric component and associated trend* uncertainties ~~errors~~*, (e, f) thermosteric*
968 *component and associated trend uncertainties* ~~errors~~*, (g,h) halosteric component and*
969 *associated trend uncertainties* ~~errors~~*, and (l, j*i *) budget residuals* and associated trend
970 uncertainties.~~errors~~

II. Sea level budget residuals of the low degree harmonics of the components

973

974 In order to highlight the contribution of the different low degree harmonics in the sea level
975 budget residuals, we decomposed each of the components, restricted to their common
976 oceanic mask, in spherical harmonics and computed the sea level budget for different
977 combinations of these low degree harmonics. The sum of all components summed up to
978 degree 4 (Figure S2~~1~~, top left panel) well reproduces the sea level budget residual map
979 characteristics with high residuals in the North Atlantic Ocean. Other panels of Figure S2~~1~~
980 show the residuals of the sea level budget with components summed up to degree 4, with one
981 harmonic signal corresponding to one (degree l, order m) combination. Table S1 provides the
982 root mean squares (RMS) for each case, computed over all oceans. Figure S2~~1~~ and Table
983 S1 show that residuals are strongly reduced in the North Atlantic Ocean when removing
984 harmonics l1m0 (geocenter term), l1m1,~~-~~ l2m1 (including the polar motion term), l3m2, l3m3
985 and l4m2. This means that these harmonics contain spurious signals in some of the sea level
986 budget components. Globally and in the North Atlantic Ocean, harmonics l1m0, l2m1 and l4m3
987 have the highest impact on the residuals.

988
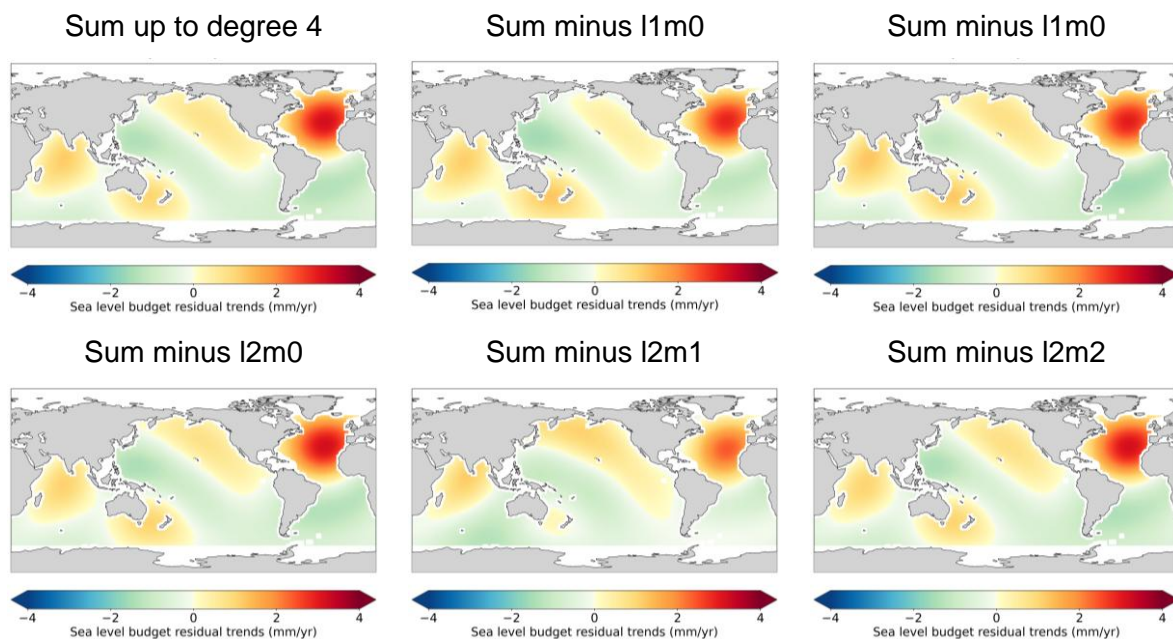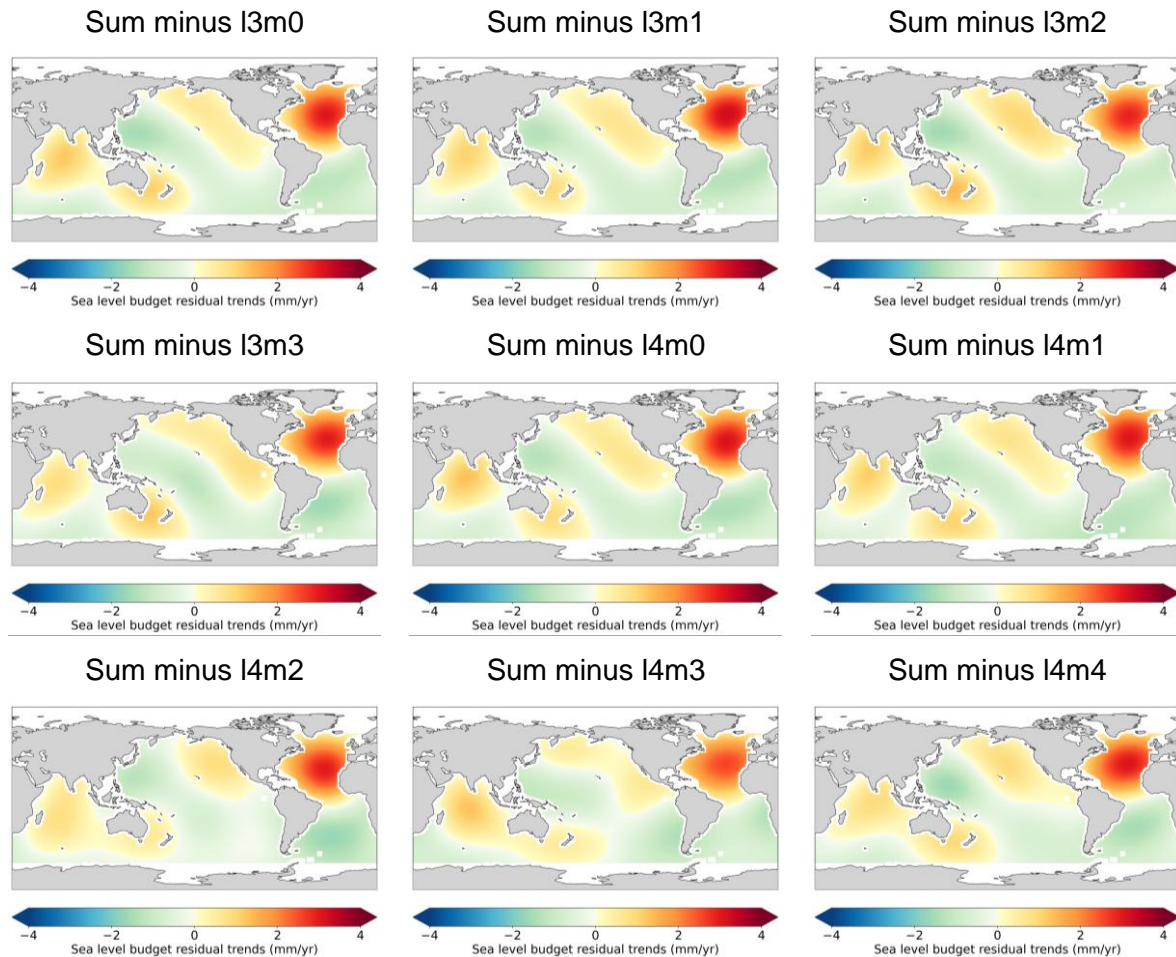
989   *Figure S2̶1̶: Sea level budget residual trends computed over January 2005 to June 2022 using*
990   *the low degrees of each component up to degree 4, and subtracting each order/degree*
991   *contribution one by one.*

992   *Table S1: Root mean square (RMS) of the residual trends computed using the low degrees of*
993   *each component up to degree 4, and subtracting each order/degree contribution one by one.*
994   *The RMS is computed over the global oceans and over the North Atlantic, South Atlantic,*
995   *Indian and Pacific Oceans. Bold font indicates RMS values which are lower than 0.1 mm/yr*
996   *below the value for the sum up to degree 4 without any subtraction (first line).*

997

Component removed from the sum of all components up to degree 4	Residual trends RMS over oceans (mm/yr)				
	Global	North Atlantic	South Atlantic	Indian	Pacific
None	0.94	2.11	1.00	0.55	0.64
l1m0	0.87	**1.86**	**0.87**	0.54	0.65
l1m1	0.92	**1.91**	1.18	0.60	0.60
l2m0	0.94	2.11	0.99	0.51	0.65
l2m1	**0.74**	**1.50**	**0.48**	0.69	0.56

l2m2	0.93	2.08	0.96	0.51	0.64
l3m0	0.92	2.01	0.92	0.59	0.64
l3m1	0.93	2.13	0.98	0.50	0.61
l3m2	0.93	**1.93**	**0.76**	0.58	0.76
l3m3	0.90	**1.95**	1.04	0.46	0.63
l4m0	0.94	2.08	1.04	0.61	0.62
l4m1	0.91	2.03	0.97	0.52	0.61
l4m2	0.90	2.03	1.16	**0.43**	**0.52**
l4m3	0.84	**1.80**	**0.80**	0.64	0.57
l4m4	0.93	2.07	1.03	0.47	0.65

III. EOF Decomposition of the gridded residual time series (with the GRACE SH-based manometric component)
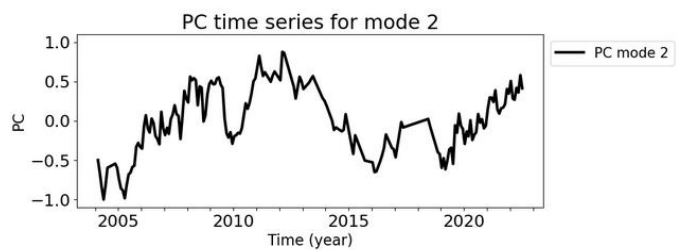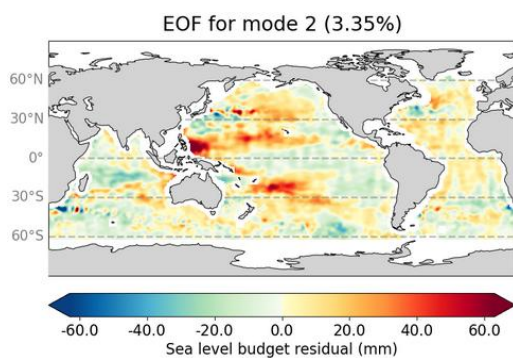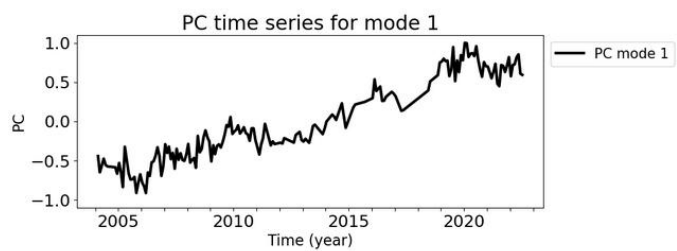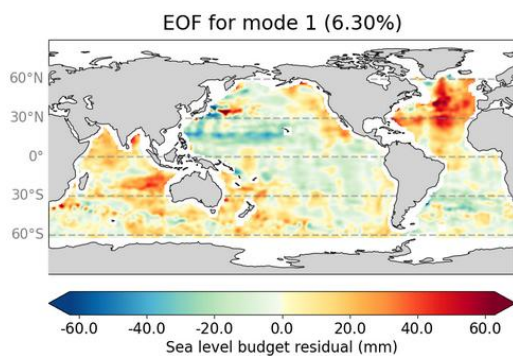
1027   *Figure S3: Modes 1 and 2 of the EOF decomposition over 2004-2022 of the gridded residual*
1028   *time series (with the GRACE SH manometric component). The left panels are the spatial*
1029   *maps while the right panels are the associated principal components (PC).*
1030
1031